Transport Research Laboratory
Creating the future of transport

JACOBS



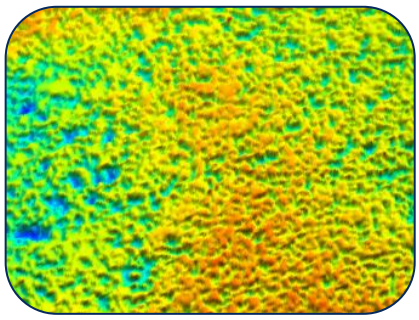

PUBLISHED PROJECT REPORT PPR643

Detection of changes in pavement texture condition using high resolution 3D surface measurements

Research into pavement surface disintegration: Phase 2 - Task 2

McRobbie, S; Iaquinta, J; Kennedy, J; Wright, A

McRobbie, Iaquinta, Wright – Transport Research Laboratory

Kennedy – Jacobs Engineering UK Ltd

Prepared for: Jacobs Engineering UK Ltd,

Project Ref: HA Ref No - 527 (1308) JCBS

Quality approved:

Stuart McRobbie (Project Manager)

Jean Iaquinta (Technical Referee)

Disclaimer

Contents amendment record

This report has been amended and issued as follows:

Version	Date	Description	Editor	Technical Referee
0.1	02/10/12	Initial draft for internal review	SMcR	JI
0.2	30/11/12	Initial draft for Jacobs and client review	SMcR	JI
1.0	13/02/13	Final version for release to client	SMcR	JI

Contents

Summary

Surface disintegration is a term used to refer to a range of progressive pavement surface defects such as fretting or ravelling. The defect results in the removal of aggregate from the surface course under the effect of the traffic, and can, if left untreated, lead to the removal of localised areas of the wearing course of the pavement, and the initiation of potholes. The defect is becoming increasingly important on the Highways Agency network due to a change in maintenance practice which has led to the use of more thin surfacings, and less hot rolled asphalt (HRA). An increasing proportion of these thin surfacings are now reaching an age where they are starting to show signs of deterioration. Surface disintegration progresses from initiation to failure at a faster rate on thin surfacings than on HRA pavements and so it is important to provide maintenance engineers with as much advance warning of the initiation of the defect as possible.

Previous research has developed methods for detecting surface disintegration using existing traffic-speed data collection systems. However, the resolution of the data available from such systems is such that the derived indicators are only successful in detecting the defect when it has already progressed extensively. This research has looked at the use of data at a much higher resolution than is currently available from traffic-speed surveys to identify, visually and quantitatively, surface texture changes which may be indicative of the early stages of surface disintegration.

A transportable platform was built for outdoor operation of a high-resolution 3-D surface measurement device and a procedure was developed for data collection. A number of derived statistical parameters potentially able to reflect changes in surface condition, or distinguish between surfaces of different types, were considered.

Visual examination of measured 3-D surface data collected using the high-resolution system on sound and deteriorated pavements showed that areas of surface disintegration could be visually identified. Additionally it was possible, when looking at data from repeated surveys on the same site, to identify areas where surface disintegration had been artificially induced between surveys by removing particles of aggregate.

Some of the quantitative parameters calculated using the measured 3-D surface data proved sensitive to small changes in asphalt surfaces where the surface disintegration had been introduced by manually removing individual stones or adding sand. Some very encouraging results derived from a principal component analysis are also presented and discussed.

The use of high-resolution data to detect the early signs of surface disintegration appears encouraging, and could provide engineers with more notice that a surface is about to disintegrate. This would enable planned, rather than reactive, maintenance to take place, which is more efficient and less disruptive.

Recommendations are made to investigate the use of such measurements in controlled conditions. This will develop our understanding of the deterioration mechanisms and the measurement sensitivities required to detect the early signs of deterioration, and will be invaluable in defining minimum requirements for a data collection system suitable for inclusion in a future TRACS contract.

1 Introduction

Surface disintegration is growing in importance as a defect of concern on the Highways Agency network (Hall, et al., 2001). This defect, also referred to as fretting or ravelling, results in the aggregate in the surface being removed from the binder, often as a result of trafficking (Figure 1). The occurrence of fretting increases with the age of the pavement as the binder ages and turns more brittle. Left unchecked, fretting can rapidly remove the top surface from the pavement, turn into potholes, and allow water into the lower layers where it can cause serious structural damage (Scott, et al., 2008).

Figure 1: Example of surface disintegration on hot rolled asphalt.

The Highways Agency made a decision a number of years ago to change its strategy with regard to surface materials used on its network. This has resulted in a change in the composition of the network with fewer hot rolled asphalt (HRA) surfaces, and an increasing proportion of thin surfacing materials being used. Many of these thin surfacings are now reaching an age where binder integrity is failing, and surface disintegration is becoming more likely. Adding to the problem is that, while fretting on HRA surfaces tends to progress reasonably slowly, with a relatively gradual deterioration from the point at which the defect first became apparent to failure of the surface course, thin surfacings have a different deterioration mechanism and a much shorter time between the onset of visible signs of deterioration to the failure of the wearing course.

Measurement techniques and algorithms have been developed over a number of years to try to detect the signs of surface disintegration. These aim to identify those parts of the network showing signs of surface disintegration, but do not give sufficient advance warning on thin surfacings for the engineer to plan a maintenance programme which will efficiently repair the pavement at the optimal time. This results in the need for reactive rather than planned maintenance, which is more disruptive and less efficient. Being able to act and prevent the defect reaching a stage where the lower levels of the pavement are compromised would be useful (Department for Transport, 2012).

The Highways Agency has commenced a programme of work to enhance the ability to detect surface disintegration. This has been undertaken in stages. The initial work aimed to enhance the performance of the method used in TRACS surveys to detect surface disintegration at the network level. More recently the work has investigated the use of high-resolution data to detect the early signs of change in a surface which may be indicative of the onset of surface disintegration.

The research into the development of algorithms to detect surface disintegration in TRACS has been reported elsewhere (McRobbie, et al., 2012). This report presents the results of research and development carried out into a methodology to enable the detection of the early signs of surface disintegration.

2 Previous work

The automated identification of surface disintegration was introduced in the first Highways Agency TRAffic-speed Condition Survey (TRACS1) contract, with the "TRACS fretting" parameter. The approach was based on a single line texture measurement in the wheel-path and an algorithm derived from the Dutch "Stoneway" algorithm (van Ooijen, et al., 2004), tuned for use on Hot Rolled Asphalt (HRA). This parameter continued to be reported throughout the TRACS2 contract. However, it has been found that the parameter does not provide engineers the information they need to determine the extent of fretting present. This is because the measurement is restricted to the nearside wheelpath, and to one surface type only. As a result engineers still rely on visual condition surveys. Unfortunately, these are not always performed in a controlled or consistent way, and often include a number of other defects which the inspector must look for and record. This can result in inconsistencies in the interpretation and reporting of different severities of the defect. Failure to detect and report the early signs of disintegration can lead to more expensive repairs later or incorrect prioritisation of the wrong sites. It is therefore important to ensure that surface disintegration is properly detected and reported and that maintenance is undertaken in the most appropriate locations.

Work was therefore undertaken to develop a new, network level, surface-type-independent method for detecting surface disintegration which uses data collected across the full width of the carriageway (Scott, et al., 2008), (McRobbie, et al., 2008), (McRobbie, et al., 2010), (McRobbie, et al., 2011), (McRobbie, et al., 2012).

Although significant progress has been made into the development of a network level measure of surface disintegration, the measure will only assist engineers in identifying the defect once it has reached a relatively advanced level of severity. Because surface disintegration can rapidly increase in severity once it has appeared, the network level measure may highlight the presence of the defect only a short time before treatment is required. Clearly it would be desirable to have a method able to identify the defect in its earlier stages to enable better planning and timetabling of treatments.

A review of how this could be achieved considered the visual appearance of surface disintegration in its early stages, and established that traditional profiling techniques would be inadequate for collection of data at the required resolutions (Iaquinta, et al., 2008), (McRobbie, et al., 2011). It was concluded that it would be more practical to achieve the detection of surface disintegration in its early stages by identifying the change in the surface shape, i.e. observing when stones have been lost by comparison with the surface before the loss.

This review process also considered a range of commercially available 3-D measurement systems which were thought to have the potential to deliver data at the resolution required to detect change. As a result of this, a Breuckmann SmartSCAN HE system was procured by TRL on behalf of the Highways Agency.

The Breuckmann SmartSCAN system is a stereo-imaging device with a structured light projector and two high resolution digital cameras (2448×2048 pixels). Data must be collected from a static imaging position, with individual images covering an area of approximately $1m^2$. The system delivers a horizontal point spacing of 400µm and a resolution of 20µm along the vertical direction (example in Figure 2).

The collection process involves projecting a series of light patterns onto the surface, and taking images of the illuminated scene. Because the geometry of the system is known, as are the projected patterns of light, the system is able to extract 3-D data from the images by calculating how the observed patterns differ from the 'expected' ones if they were taken on a flat plane.

By assigning a colour, based on the measured profile height, to each measured point in the surface it is possible to produce pseudo-colour 3-D models which can be used to visualise how the surface texture varies across the measured area (Figure 2).

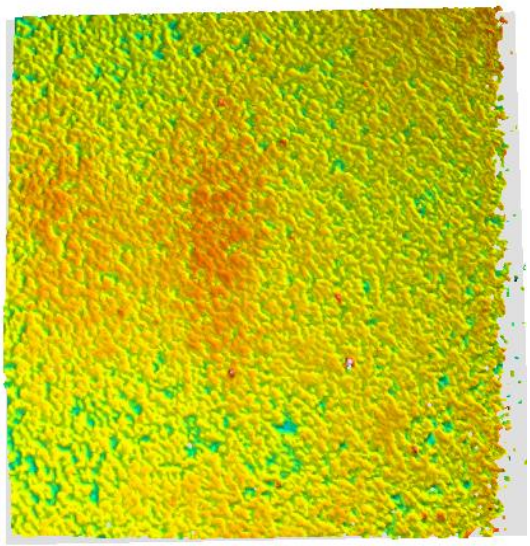

Figure 2: Approximately 1m^2 of high resolution data as used to investigate the detection of small changes in pavement surface material.

The Breuckmann system was tested in initial work carried out by McRobbie, et al., (2011). The work showed that it should be possible to measure surfaces to a resolution that might allow the detection of change. However, the work recommended that improvements be made to the collection system to allow data to be collected on a larger range of sites to deliver 3-D data that could be used to support the development of algorithms for the detection of change. The work presented in this report has focussed on these developments.

The Breuckmann system was procured in the belief that the data it produces is at a higher resolution than that which will be required for the traffic–speed implementation of surface disintegration algorithms. Consideration of such high-resolution data will help to develop the understanding of the physical changes which become apparent on the pavement in the presence of surface disintegration, which will in turn help to inform the subsequent decisions on what data resolution would be acceptable from a traffic-speed system, and how such data may be processed and interpreted.

3 Methodology

This section provides details about the development of a mobile platform for the Breuckmann SmartSCAN HE that would allow larger quantities of data to be collected. We also describe the approach taken for the collection and analysis of the data, and the sites chosen for inclusion in the study.

3.1 System mounting platform

The Breuckmann SmartSCAN HE system (Figure 3) has to be static so as to ensure an optimal data capture. This is because up to 11 different light patterns are successively projected on the area under inspection to work out the 3-D information of the scene while a series of images are collected. The scene must not change during the collection of the images. It takes approximately one second to perform the scan, then a few more seconds for the processing and extraction of 3-D data from the images. There is no way to operate the system whilst moving without a significant degradation of the measurements.

Figure 3: Breuckmann SmartSCAN HE system with its two camera on either side of the beam and the lighting unit in the centre.

Initial work to establish the capabilities of the SmartSCAN HE system (McRobbie, et al., 2011) used a set-up where it was mounted on a tripod and pointed down (as shown in Figure 4) to optimise the ability to measure the full extent of the surface texture depth.

Figure 4: Breuckmann SmartSCAN HE system mounted on tripod with the lighting unit projecting various patterns.

Such an arrangement was, however, not practical for large scale data collection. It was also found that the data acquisition only performed well in low light conditions, implying that the area being scanned had to be shielded from as much light as possible.

Therefore the constraints on developing a "mobile" platform were that each image had to be collected statically, and in controlled lighting conditions. This resulted in a final design for the mounting platform in which the camera is 1.5m above the ground, levelled horizontally, and pointing vertically downwards (the precise location of the system can be adjusted by sliding the mounting bar along the side arms of the platform). The system has walls and a ceiling made of darkroom material and fastened using Velcro strips which can be detached to allow access to the device. Four wheels are used, two of which are lockable. These wheels are placed outside the main body of the enclosure so as to rotate fully and not impinge on the area being studied. A handle aids moving the platform from location to location, and the entire system can fit into the back of a van, for transport to site without requiring a rebuild of the platform before use. Photographs of the mobile mounting platform for the system are shown in Figure 5 and Figure 6.

Figure 5: Mobile mounting platform with side panels partially opened (left) and closed (right).

Figure 6: SmartSCAN system installed inside the mobile platform.

The camera, projector and associated control boxes require 240V power. In a laboratory this can be obtained easily using the mains supply, but on site this has to be provided via a generator. It is preferable if the generator is sited so that vibrations do not affect the platform or surface being studied. This can be achieved by putting the generator in a vehicle which can be positioned alongside the survey platform.

3.2 Sites

The criteria for the sites to be used in the work were that they had to be easy to get to with the equipment, easy to work on safely, in a variety of conditions, and in locations where the surface could be marked or altered in some way. A number of sites were identified on and around TRL premises (Figure 7 and Table 1).

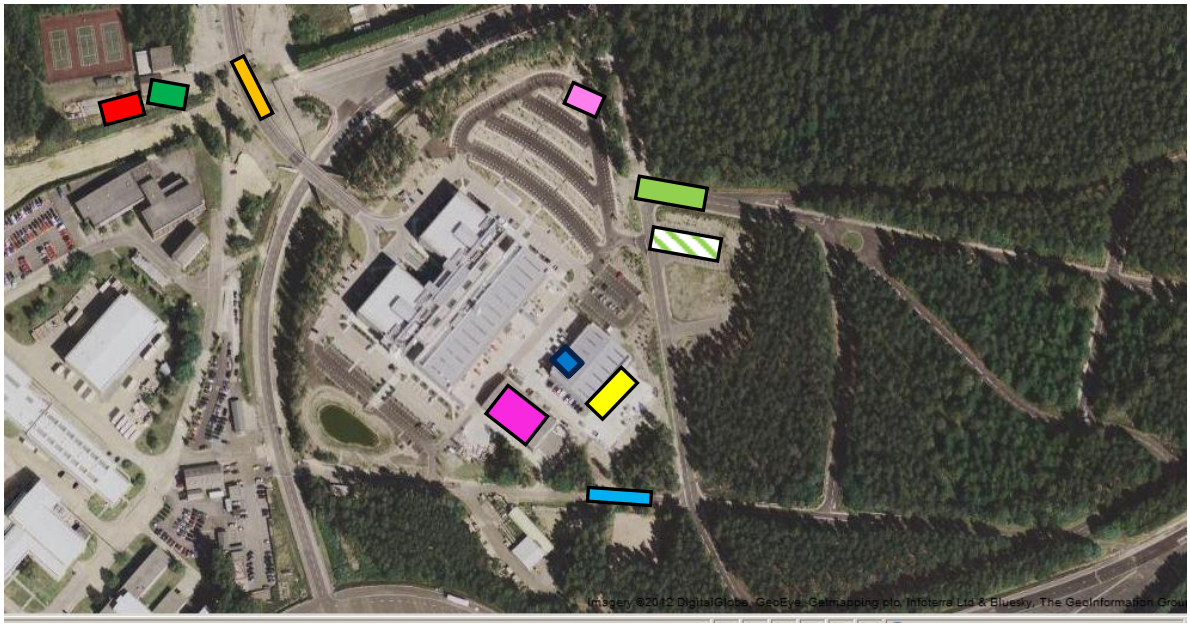

Figure 7: Various sites considered in this study.

Table 1: Details for potential sites on TRL's premises (only those numbered are discussed in this document).

Site ID	Location	Surface	Condition (initial)
0	Garage	Smooth finished concrete	0 – Smooth concrete surface with a few minor scratches
1	Small Road System access	HRA	1/2
2	Near tennis courts	HRA/TS	2/3 – Old and poor condition HRA, with completely loose aggregate in some places.
3	Staff car park	TS	0
4	Near social club	HRA	2/3 - Old and poor condition HRA
	Small Road System car park	TS	0/1 – mainly good condition, with a few areas of fretting
	Small Road System	TS	0/1 – mainly good condition, with a few areas of fretting
	Rear of the garage	Concrete	0/1 – Generally sound
	Pavement testing Facility	Various	0/1/2 – pavements were rutted and cracked, but generally little or no surface disintegration was present
	Cycle path	TS	0-2 in places

3.3 Data collection, processing and alignment

The data collection, pre-processing and alignment were undertaken with proprietary software which had been supplied with the hardware. The analysis was largely performed using another commercially available software package.

Most of the quantitative data analysis was carried out on individual 3-D image data. However, it was also useful to merge data from individual scans to create a larger dataset. For this purpose the data collection procedure needed some way of identifying which parts of any given scan matched which parts of the neighbouring scans.

The software used is able to translate and rotate a scan relative to another one after having identified reference points within the datasets considered. This can either be achieved automatically, using markers, or by manually selecting points corresponding to the same point within each dataset. The automated feature matching approach, using markers, was discarded since it would result in artificial features being present within the data, which could be hiding areas of interest. The manual method is slightly more labour intensive, but it can either be done on-site while the data is being collected, or off-site as part of a re-processing procedure. In order to perform this manual identification of control points there had to be a number of them in both data sets which could be unambiguously identified as being from the same place on the pavement. Unfortunately in the unadulterated scans of a pavement surface it proved very difficult to identify in two scans any stone as definitely being the same. To help with this process features have to be present in all the scans.

It was found that a practical solution was to draw a wiggly chalk line on the surface of the pavement being surveyed. The 2-D image data could be used to unambiguously align the scans, but because the chalk line was itself 2-D it did not affect the measured texture. This meant that parameters could be derived on the each individual dataset, but also that successive surveys could be compared to detect changes in the surfacing, with confidence that the same piece of pavement was considered.

Figure 8 shows the way in which the system was moved from collection point to collection point (moving the collection platform from location to location, along the track marked out by the lines drawn on the surface, each move being less than the length of pavement included in each measured profile to ensure sufficient overlap).

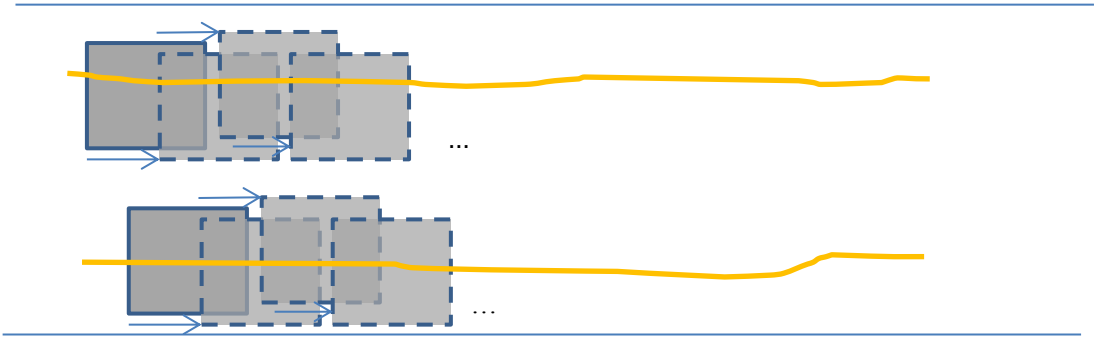

Figure 8: Principle of the data collection following lines drawn on the pavement to facilitate the alignment of the individual images.

The overall data collection and processing workflow is illustrated in Figure 10.

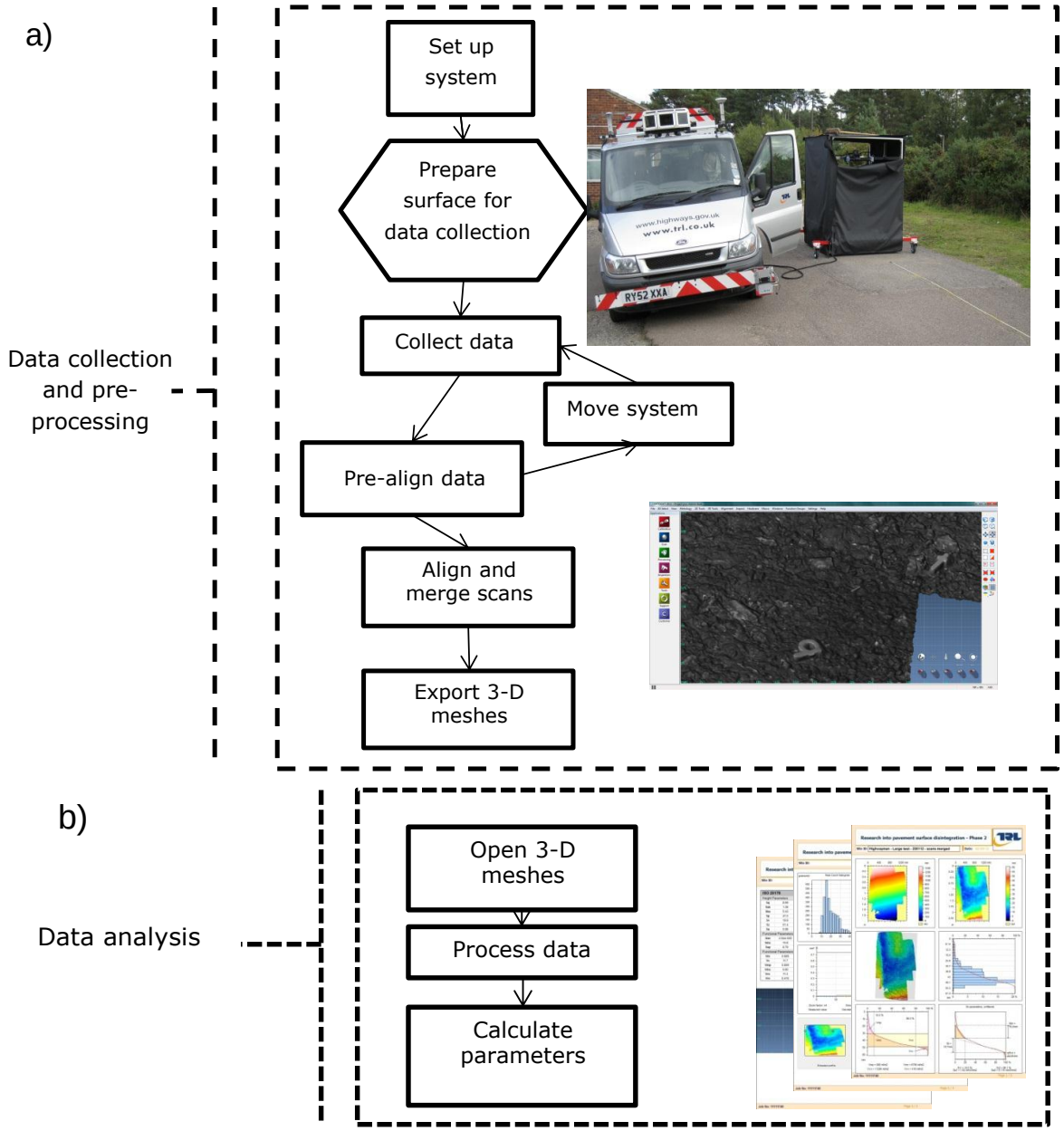

Figure 9: Workflow for a) collecting and pre-processing, b) analysis of the 3-D data.

Data was collected on each site following initial preparation which included sweeping off debris (except for Site 2, in Section 4.2.4), measuring and marking of the site. Where possible and practical the condition of the surface was then altered, at least in some locations, before data was collected again. This was done in order to determine whether the introduced changes could be detected, either qualitatively or quantitatively. The changes sometimes involved the removal of texture depth by adding fine sand to fill the voids and sometimes the removal of aggregate.

Some of the sites discussed in this document were surveyed on several occasions, with the condition changing between the surveys. A summary of the different survey files referred to in this report is given below in Table 2.

Table 2: Summary of survey files and site condition.

Survey file name	Condition
0	As found
1a	As found
1b	Sand added to reduce surface texture in places
2a, 2b, 2c	As found
2d	Aggregate removed to increase texture in places
3a	As found
3b	Aggregate removed to simulate surface disintegration in small patches
4	As found

4 High resolution 3-D measurements

The data recorded by the SmartSCAN HE system can be displayed as a pair of stereo-images (without additional processing) or 3-D surfaces (that is a digital elevation model where the height of each points was calculated). It can be studied more quantitatively by extracting statistical quantities from the 3-D data. This section presents examples of the types of images obtainable from the system to demonstrate the level of detail available, and provide some scale and context for the images, before addressing specific questions which the research is trying to answer: can differences and changes in surfaces be detected visually, and, if so, can these differences and changes be quantified.

4.1 Example

Figure 10 shows a screenshot of the data-processing software, with an overview of the area of pavement surveyed with the SmartSCAN HE. The image on the left is a composite of seven individual scans. At this scale the appearance is similar to what an inspector performing a walked visual survey would normally see (i.e., dark features on a dark background), and it is possible to spot defects and areas where the surface is different from its surroundings.

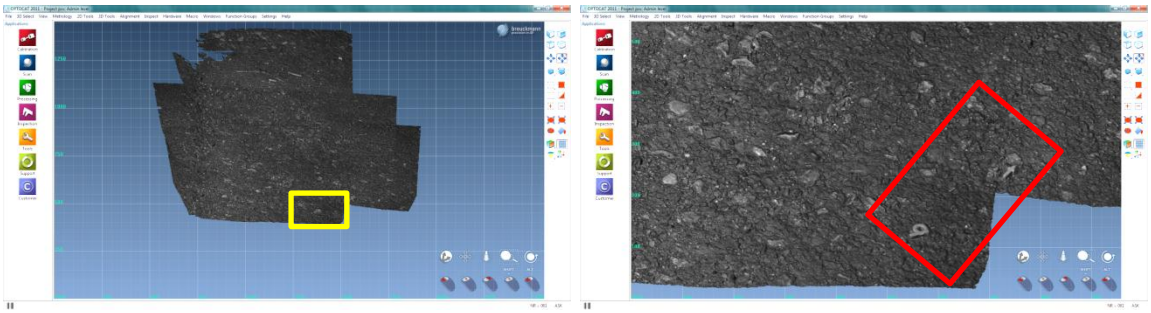

Figure 10: Screenshot showing 7 merged scans (left), and a close up of the area highlighted in yellow rectangle (right).

The image on the right of Figure 10 is a screenshot of the same dataset, having zoomed in to the area picked out by the yellow rectangle shown in the left image. This is a much closer view of the pavement, in which some of the individual stones and objects on the pavement surface can be distinguished.

Figure 11 presents a closer view of the part of the data highlighted by the red rectangle in the image of Figure 10. In Figure 11 it is clearly possible to pick out individual stones and resolve small features. The yellow ellipse on the picture highlights a plastic fridge magnet, in the shape of the letter 't', which was placed on the pavement prior to data being collected to aid the alignment of the different datasets. This same object is also shown in Figure 12 along with a ruler to provide an indication of the scale (i.e. the object is approximately 43mm long and 9mm wide).

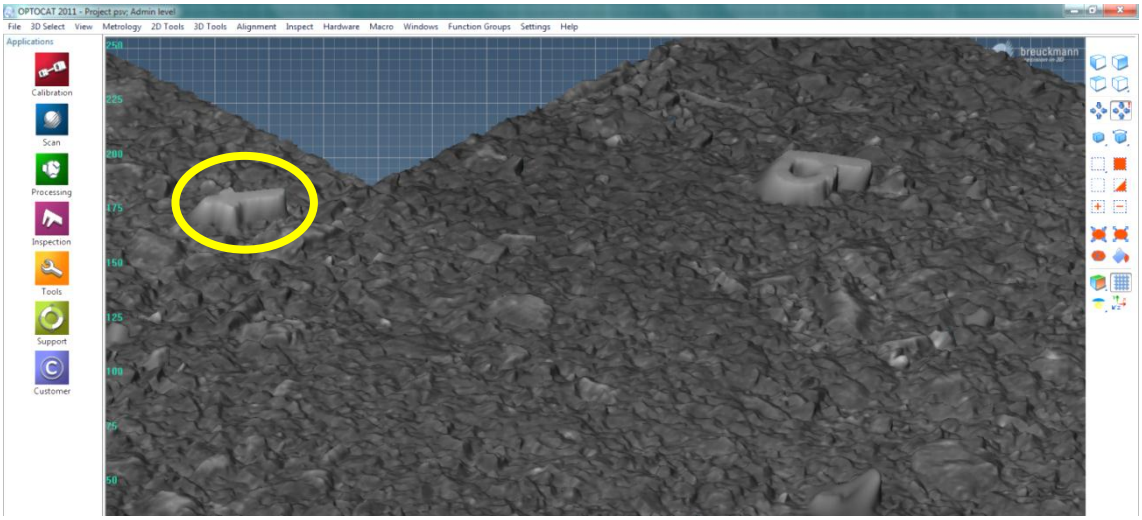

Figure 11: Further close up and rotation of data shown in Figure 10.

Figure 12: Photograph showing one of the objects placed on pavement in Figure 11, with a ruler for scale.

Figure 13 is an example screenshot showing the distance measurement facility within the analysis software. The measured length of the 't' shaped fridge magnet is 42.9mm, which agrees well with its actual size.

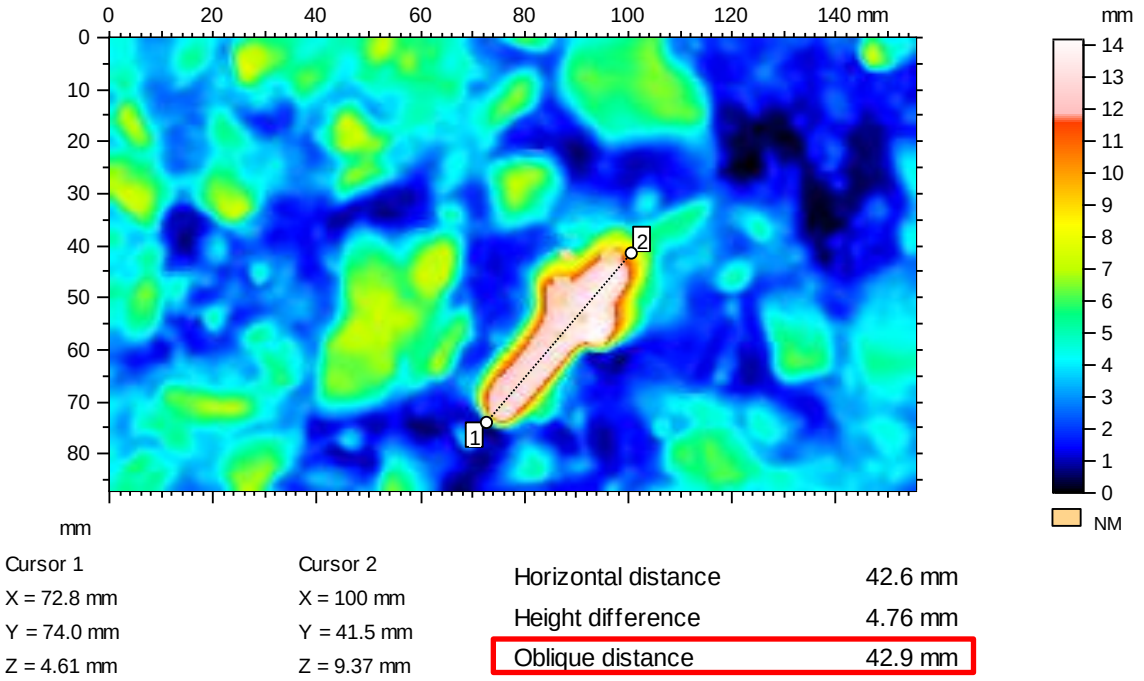

Figure 13: Screenshot showing distance measurement on a scanned 3-D surface ('NM' means 'Not Measured' and is for points where the triangulation failed).

Figure 14 presents an example of image of a pavement surface in which different measured surface heights have been colour coded, including axes with the scale of the measured area and a summary of the dimensions of the measured area. In this case the area is 905mm × 868mm and the height difference between the highest and lowest points in the data represents 26.9mm.

Note that colour scale bars only apply to a particular plot: this is because the choice of the colours has been optimised for each surface in this report. Accordingly the measured height difference between a red point and a blue point will be different for each image.

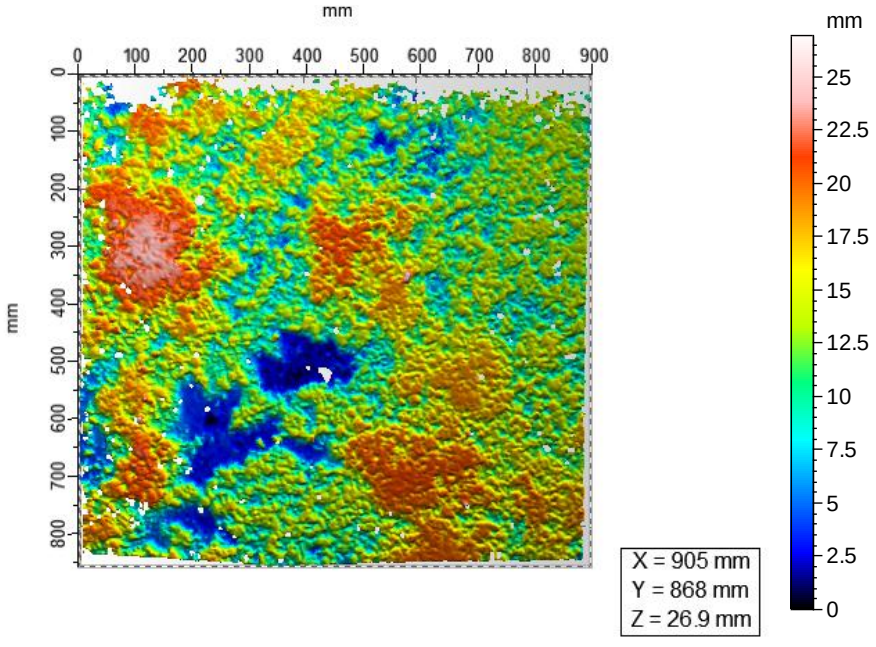

Figure 14: Example of 3-D data, showing dimensions of measured area

4.2 Subjective visual detection of change

The Breuckmann SmartSCAN HE was used on various pavements exhibiting different conditions. Before proceeding with the quantitative analysis of this data the 3-D images were examined to establish whether it was possible to visually and subjectively discriminate between these surfaces.

4.2.1 Atypical surfaces

Some of the initial testing and calibration of the Breuckmann SmartSCAN HE system was performed on a concrete garage floor (Site 0). This had the advantage of being indoors, in a controlled environment where traffic, power and weather conditions were not an issue.

Figure 15, Figure 16 and Figure 17 display examples of photographic images and data obtained from the Breuckmann SmartSCAN HE. The area shown in each image (the left hand side of each figure) and surface (the right hand side of each Figure) is the same in size in all cases, and the field of view is approximately 900mm×900mm.

Figure 15 shows part of the garage floor on Site 0 where striped tape has been used to delimit vehicle parking space. The tape is clearly visible in both the image and the 3-D surface. Also visible are a bright spot where the projector light was shining, a tyre mark towards the top of the image, and a number of small irregularities in the surface, such as the indentation (probably the result of a heavy object dropped on the floor) highlighted by a purple circle on the figure. This is also noticeable in the image on the left as a small bright spot (highlighted with a yellow circle) where the light has caught the edge of the indentation.

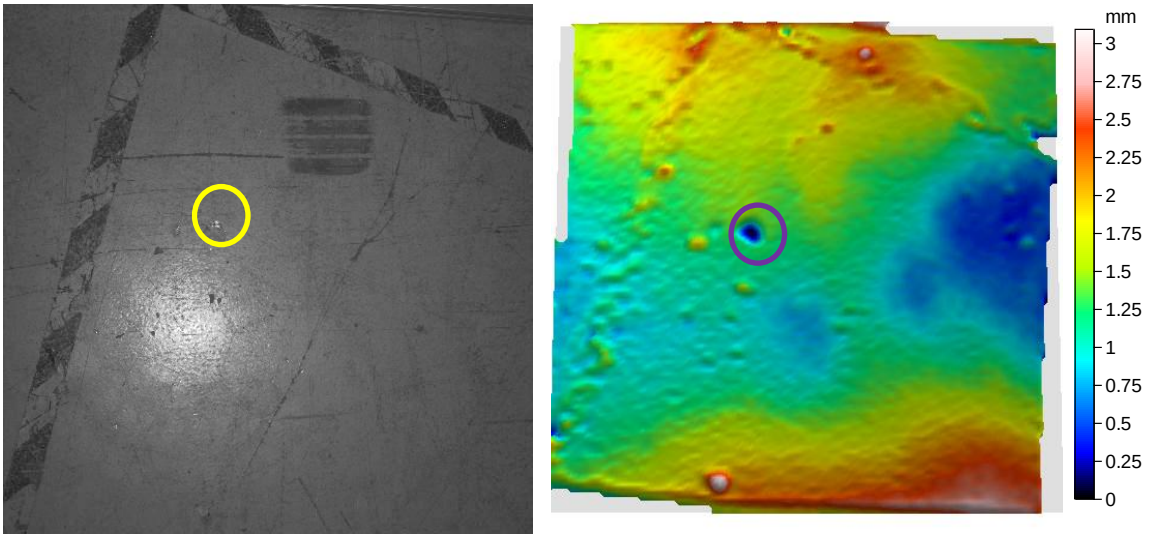

Figure 15: Example image (left) and 3-D surface (right) collected on a garage floor.

Analysis of the surface profiles extracted from the data in Figure 15 suggests that the measured height profile of the tape is between 250 and 300µm.

Figure 16 corresponds to data collected on another area of the same garage floor which has been treated with a special material to produce a much smoother surface. There is much less variation in the profile, with more consistent surface heights exhibiting only slight changes (in the range of ±8.5µm). There is a small feature visible in the 3-D data towards the bottom of the data, which can also be seen in the image. Also visible around

the upper edge in the 3-D data is a pattern of lines which is thought to be an artefact introduced by movements/vibrations of the measurement system during acquisition. Although the measurement platform was carefully positioned following the developed procedure, and the wheels were locked in place, there were other vehicles operating in the vicinity at the same time. This highlights the need for data acquisition in a vibration-free environment.

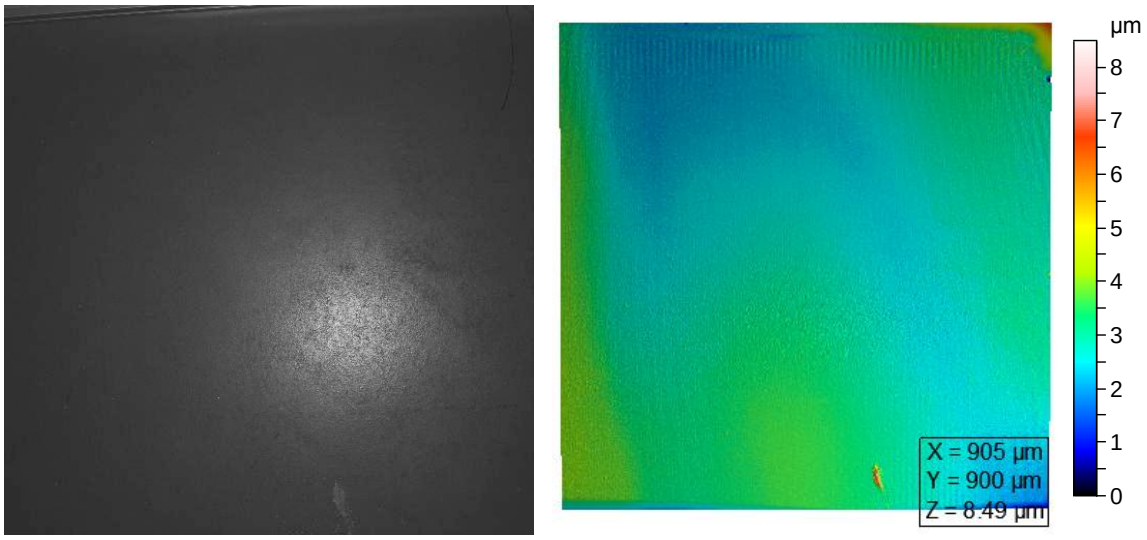

Figure 16: Example image and 3-D data from the smooth garage floor area.

The example in Figure 17 shows data collected on a metal mat on which square waves with known characteristics (25mm width and 1.5mm depth) have been machined. This mat is normally used for the accreditation of laser profilers. As well as the mat texture pattern the joint in the floor upon which it was laid stands out in both the image and the 3-D surface. Data from an extracted 2-D profile measured on part of the mat is plotted in Figure 18.

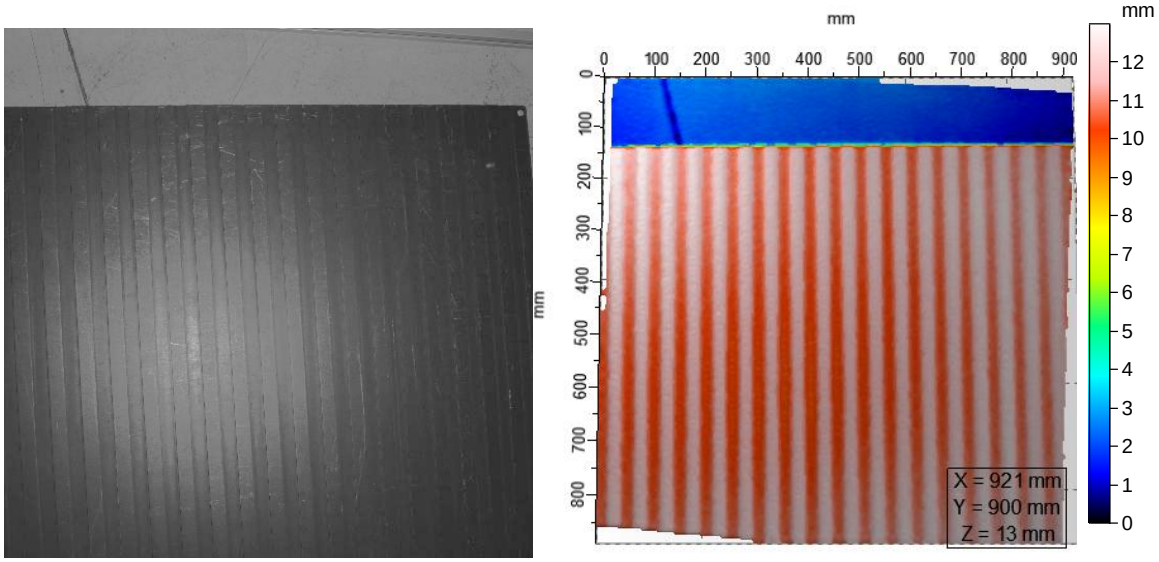

Figure 17: Example image and 3-D data from textured mat.

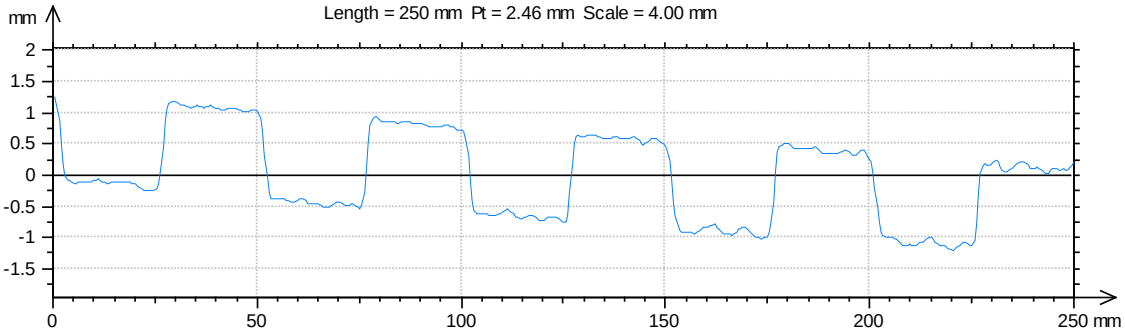

Figure 18: Transverse profile of part of the textured mat shown in Figure 17.

The profile in Figure 18 follows the square wave pattern which has been milled into the metal. The amplitude of the measured profile is 1.5mm, and the wavelength is 25mm. The transitions from maxima to minima are very sharply defined.

Data and images from three different artificial surfaces with small texture features (a few mm in height) have been shown in Figure 15, Figure 16 and Figure 17. The measured surfaces are clearly different from one another, and it is easy to identify which surfaces are smoother and more consistent than others, and to identify features and patterns in the data. This gave us confidence that the system was very likely to perform similarly on actual pavement surfaces.

4.2.2 Pavement surface - No change in texture

The image (on the left) and 3-D surface data (right) shown in Figure 19 and Figure 20 are from approximately the same location in Site 3 (note chalk marks). The two survey runs were performed one after the other, within the same afternoon, without any trafficking of the pavement by vehicles taking place between surveys, so there should be no appreciable change in the condition of the surface measured in each pass.

Visual examination of the surface data presented in Figure 19 and Figure 20 reveals very little difference in the measured surfaces, although it is possible to pick out a number of features present in both. This subjective comparison suggests that 3-D surfaces recorded using the SmartSCAN HE system are consistent when the object/target has not been altered, and accordingly any change in the data is probably genuine.

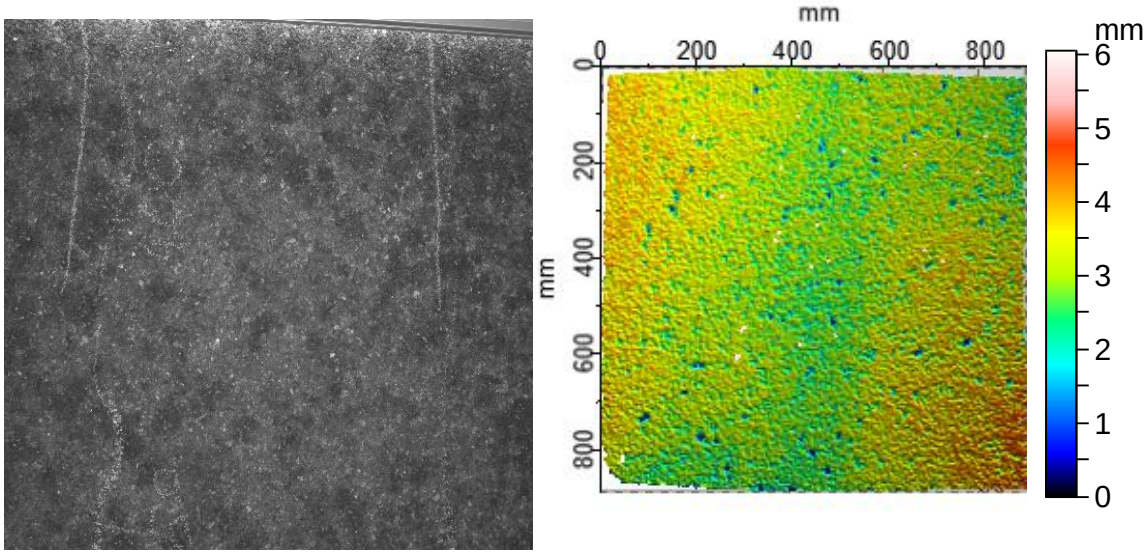

Figure 19: Example of image and surface from Site 3, survey run A.

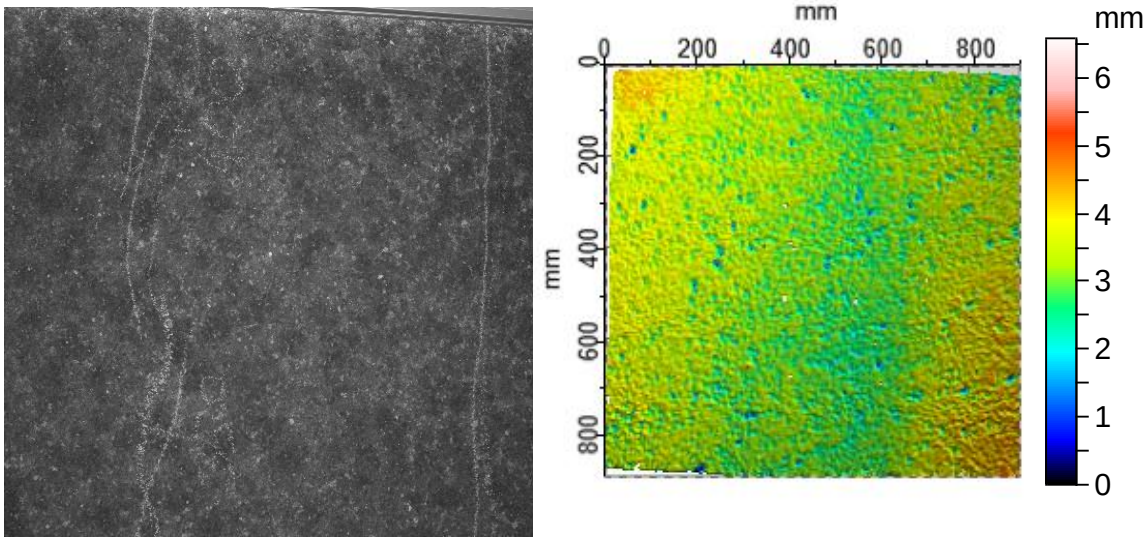

Figure 20: Example of image and surface from Site 3, survey run B.

4.2.3 Pavement surface - Removal of texture

Figure 21 and Figure 22 also show image and surface data from about the same location on Site 1. The data in Figure 21 is from the pavement in its 'as-found' condition. That in Figure 22 was collected following the addition of a patch of finely textured sand which was worked into some of the pavement texture voids in order to fill these and reduce the surface texture. The measurements took place within an hour of each other, with no trafficking of the surface taking place in between the surveys.

The area where the sand has been spread can be seen very clearly in both the image and the surface data shown in Figure 22. In the image, the sand shows up as a lighter patch, and in the surface data the sand shows up as a region in which there is clearly less variation in the measured surface profile heights.

These examples demonstrate that it is possible to visually identify locations where changes to the surface occurred between successive surveys, or where the surface macro-texture decreased.

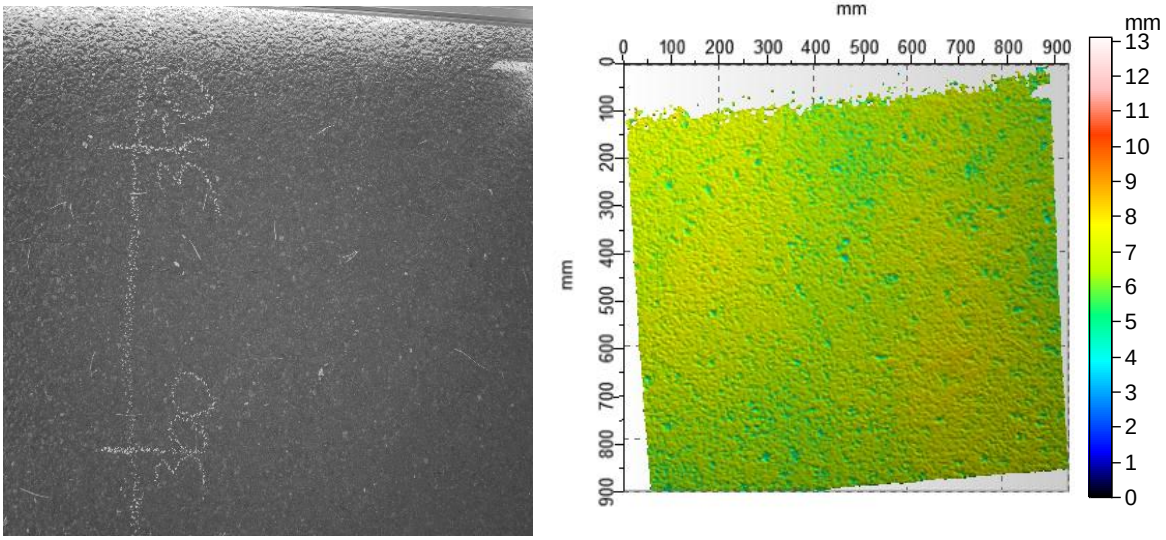

Figure 21: Example of image and surface from Site 1, survey run A.

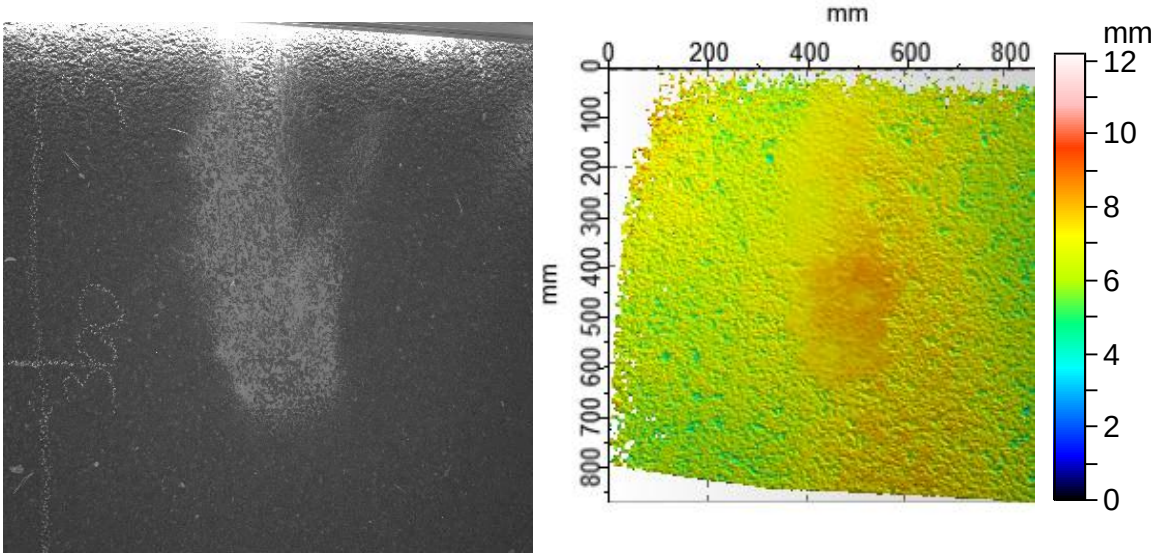

Figure 22: Example of image and surface from Site 1, survey run B.

4.2.4 Pavement surface - Removal of aggregate

The final demonstration of visual detection of changes (and the one which is most relevant to the detection of surface disintegration) is to show that it is possible to identify areas which have been affected by the removal of aggregate.

Figure 23 and Figure 24 are from two successive surveys on the same part of pavement in particularly poor condition, with loose aggregate and fretting already present. Examination of the chalk markings in the image data in the two Figures again helps to establish the overlap between the two surveys.

The data shown in Figure 23 was recorded with the pavement in an 'as-found' condition, the data in Figure 24 after removing aggregate particles from the surface.

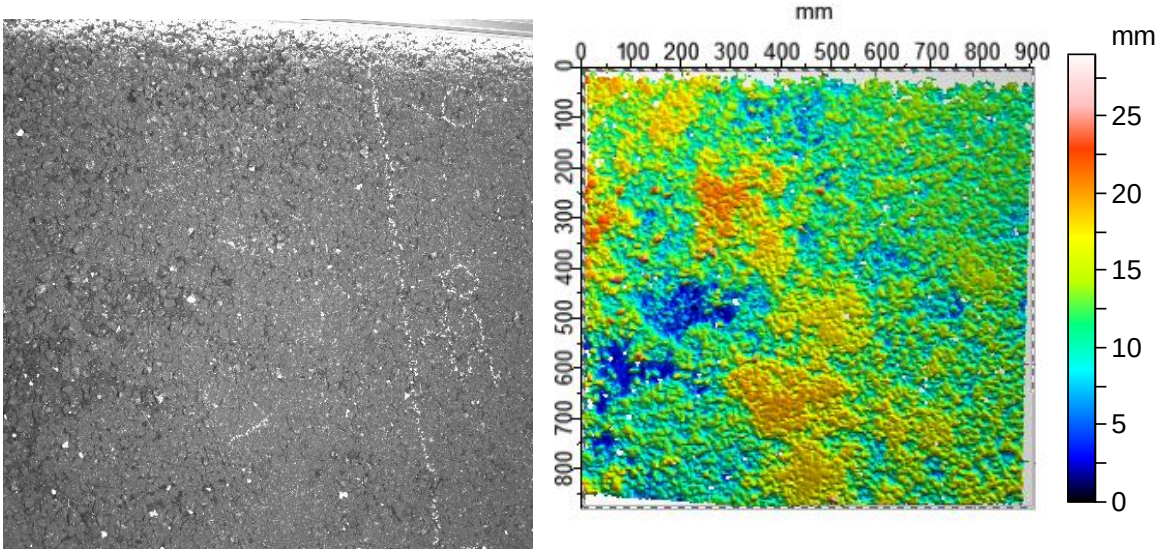

Figure 23: Example of image and surface from Site 2, survey run C.

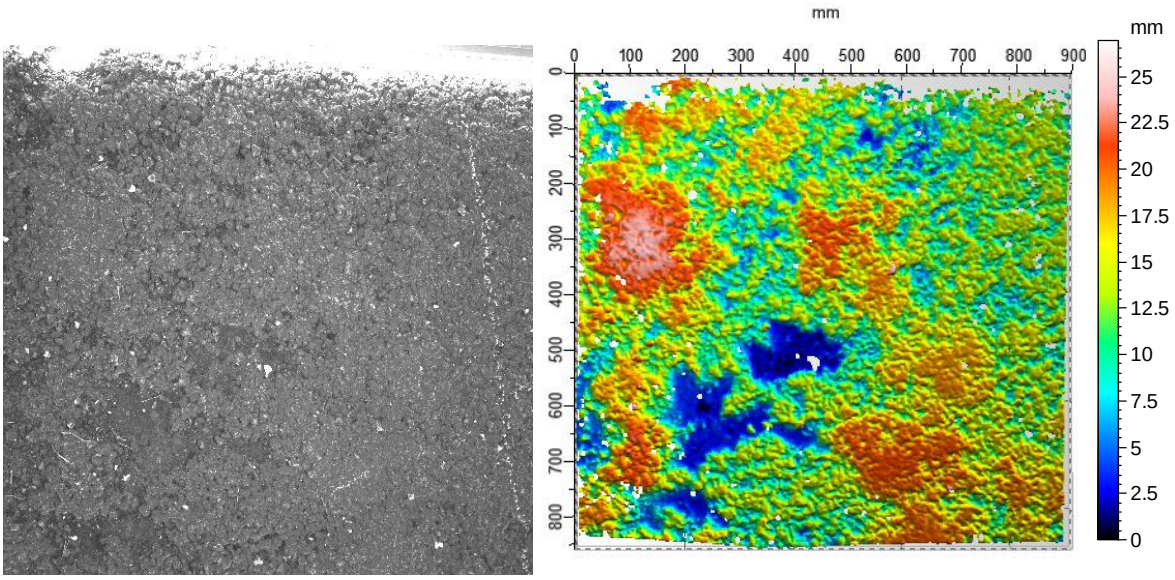

Figure 24: Example of image and surface from Site 2, survey run D.

There are a small number of obvious changes in the images after removal of aggregate. These can be seen more clearly in the 3-D data. The larger blue areas in Figure 24 correspond to places where stones were removed, resulting in a larger region with much higher texture depths.

Further tests were carried out on other pavements with different surfaces, and which were in better initial condition. Breuckmann SmartSCAN HE images and surface data from these tests are shown in Figure 25 and Figure 26.

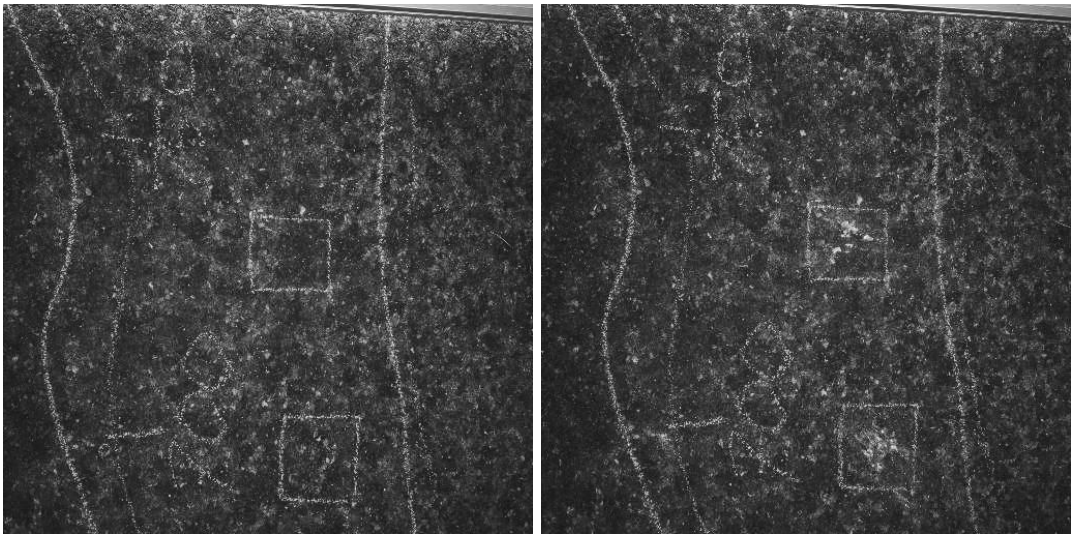

Figure 25: Breuckmann SmartSCAN HE images of pavement showing marked areas from which aggregate was removed.

Figure 25 is an example of images collected by the Breuckmann SmartSCAN HE system. The image on the left was from the pavement in its 'as-found' condition; the image on the right was recorded following the removal of aggregate from the two regions marked with the chalk squares. Figure 26 shows 3-D surface data corresponding to Figure 25. The loss of aggregate can be seen in the right-hand image, as a couple of depressions in the surface.

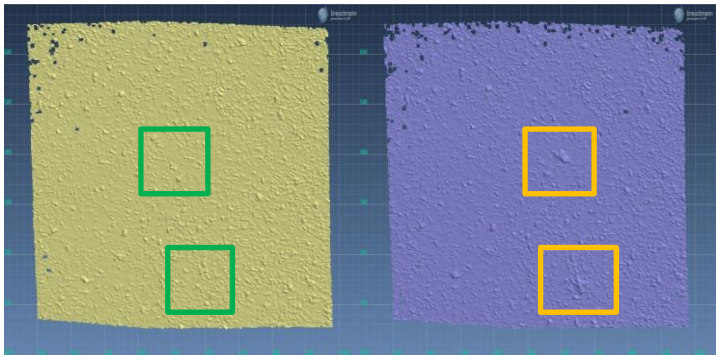

Figure 26: 3-D surface measurements from before (left) and after (right) removal of some aggregate from boxed areas.

Figure 27 shows close ups of one of the areas highlighted in Figure 26. The data shown on the left of Figure 27 was collected with the pavement in its as-found condition; the data on the right was collected after some of the aggregate was removed.

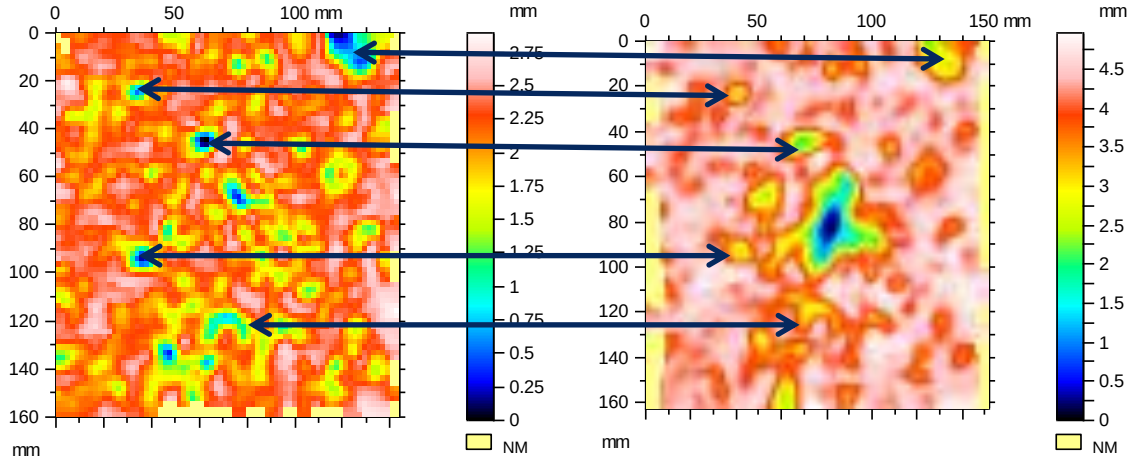

Figure 27: 'As-found' (left) and 'damaged' (right) 3-D surfaces corresponding to one of the areas highlighted in Figure 25 and Figure 26.

Despite the changes to the macro-texture in the two surfaces there are some features which can be recognised in both surfaces (arrows on Figure 27). The damaged zone is clearly visible in the 'after' surface.

Note the colour scale has changed slightly to reflect an increased texture depth in the damaged area: on the original pavement the height measurements were in the range of 0 to 3mm; the maximum measured depth increased to 5mm in the 'damaged' region.

4.3 Review of parameters for quantification of change

Although it was useful to demonstrate that changes could be seen visually within the collected images and 3-D data, this would not lead to objective or repeatable measures. The performance of a number of mathematically defined parameters, which would lead to an objective and quantitative assessment of the surface condition (or any changes therein) is now investigated.

4.3.1 Parameters

A large number of parameters are commonly calculated from 3-D surface data to characterise the shape or texture in a variety of ways. Some of these are 'surface' parameters (denoted by an initial '*S*' in the parameter name) and others are 'volume' parameters (initial '*V*'). After consultation with experts in the field of surface texture measurement a selection of parameters were chosen for further examination.

All the parameters conform to the ISO standard 25178-2 (International Organization for Standardization, 2012) or ISO 13565-2 (International Organisation for Standardization, 1997). Those used in this research are listed in Appendix A.

The selection of the final 'indicators' had to consider which parameters best described the characteristics of the surface, and which ones would work best in combination to 'condense' this information in a way to reflect different surfaces, surface conditions, and crucially, changes in surface condition.

Two of the parameters, namely *Sa* and *Vvc*, are plotted against each other (following normalisation by dividing by the standard deviation) on Figure 28.

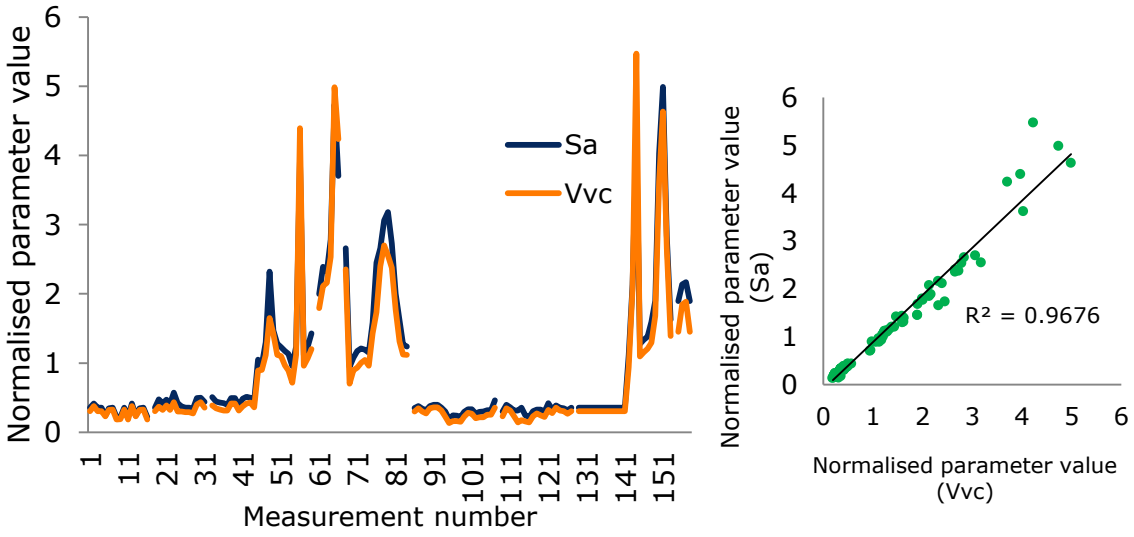

Figure 28: Plots showing strong links and correlation between the parameters *Sa* and *Vvc*.

Figure 28 shows that *Sa* and *Vvc* are very strongly correlated (with a coefficient of determination R^2 of 0.9676), which means that any change in one of the parameters is very likely to be accompanied by a change in the other one. Therefore there is no point in using both parameters to characterise a surface since almost all the information in one parameter is also present in the other, rendering it redundant.

On the other hand, parameters like c_2-c_1 and *the mean density of furrow* (Figure 29), while still linked, are not so strongly correlated with each other (R^2 value of 0.1978), and could potentially provide complementary information.

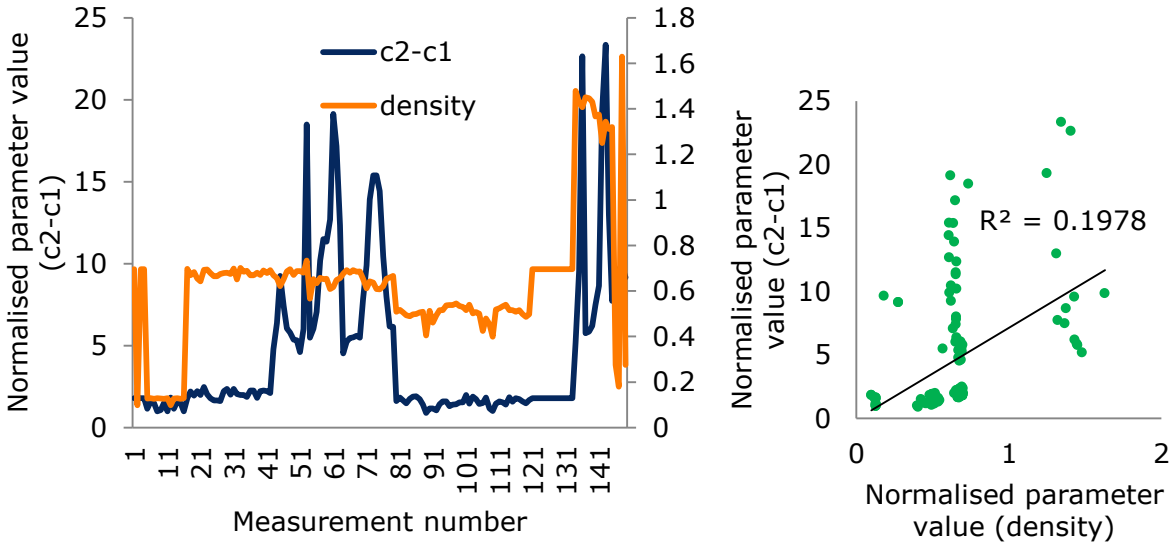

Figure 29: Plots showing weaker links and correlation between the parameters 'c_2-c_1' and '*Mean density of furrow*'.

4.3.2 Principal Component Analysis (PCA)

A procedure named Principal Component Analysis (Pearson, 1901) was applied to reduce the dimensionality of the problem and convert a large set of *possibly correlated variables* into a smaller set of *linearly uncorrelated Principal Components* (PC). In this process the first principal component (PC_1) conveys as much of the variability in the data as possible and the following components (PC_2, PC_3, etc.) exhibit the highest variance whilst being uncorrelated with the preceding ones.

A number of parameters (shown in Table 3) were calculated for various sites (listed in Table 1), and converted into 'standardized' variables (mean of zero and standard deviation of one) to calculate the principal components. This provides coefficients by which each standardized original variable should be multiplied to get the principal components (dimensionless).

For the sake of convenience only the coefficients obtained for the first three components are presented below (Table 3). This is because PC_1, PC_2 and PC_3 already account for 69.6%, 9.5% and 7.1% of the variance of the original data, respectively (more than 86% of the total).

A positive projection on to a principal component (which is the case, among others, for c_2, *Sa*, *Sk* and *Sq* on to PC_1) means that there is a strong correlation between this particular parameter and the principal component in question. A negative coefficient (*Sku* and *Smr* on to PC_1, for instance) as well as when parameters hardly project on to a principal component at all (end of Table 3 for PC_1) correspond to a weak correlation. Due to a large number of parameters the interpretation is challenging however plots of the data along with projections of the original features on to the first two or three components provide some insight (see Figure 30). Further analysis of the data may

result in a reduction of the overall number of parameters needed in the calculation of the principal components.

Table 3: Loading (or weight) matrix for the first three principal components. The values highlighted in red, green and blue provide the highest contribution to PC_1, PC_2 and PC_3, respectively.

Parameters	Coefficients for		
	PC_1	PC_2	PC_3
c_1	0.75	-0.13	0.31
c_2	**0.98**	0.24	0.12
c_2-c_1	**0.97**	0.00	0.39
Vmp	0.93	-0.23	-0.25
Vmc	**0.96**	0.43	-0.11
Vvc	**0.95**	-0.61	-0.05
Vvv	0.88	-0.77	-0.31
Sk	**0.97**	-0.32	-0.66
Spk	0.89	**0.64**	-0.06
Svk	0.82	0.16	0.17
Sr_1	0.42	0.11	-0.36
Sr_2	0.31	0.23	0.46
Sa_1	0.74	-0.54	-0.13
Sa_2	0.59	0.23	-0.12
Maximum depth of furrows	**0.96**	-0.03	-0.13
Mean depth of furrows	0.92	-0.68	0.16
Mean density of furrows	0.56	0.56	**0.76**
Wavelength	0.32	0.06	0.21
Amplitude	0.70	0.25	0.06
Sq	**0.97**	0.15	0.17
Ssk	0.54	-0.04	-0.35
Sku	-0.38	0.24	-0.09
Sp	0.95	-0.11	0.10
Sv	0.90	0.17	-0.10
Sz	**0.96**	-0.09	0.12
Sa	**0.97**	-0.40	0.02
Smr (c=1μm under highest peak)	-0.36	-0.07	0.32
Smc (p=10%)	**0.96**	0.17	0.12
Sxp (p=50%, q=97.5%)	0.93	0.17	-0.17
Vm (p=10%)	0.93	0.14	0.16
Vv (p=10%)	0.20	0.22	-0.07
Vmp (p=10%)	0.07	0.04	0.01
Vmc (p=10%, q=80%)	-0.03	0.07	-0.20
Vvc (p=10%, q=80%)	-0.09	0.29	0.24
Vvv (p=80%)	-0.02	-0.17	-0.12

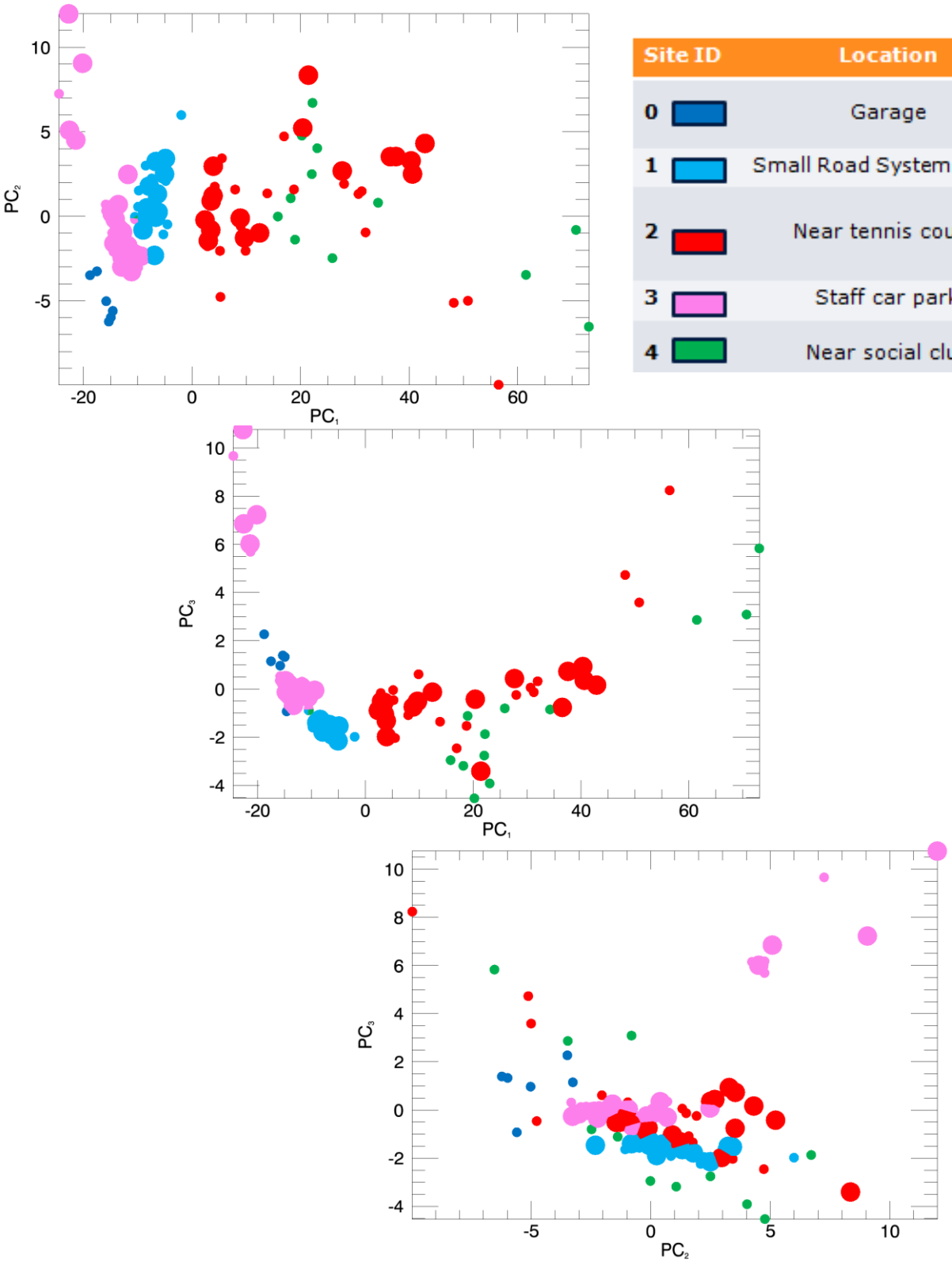

Figure 30: Bi-plots with PC_2 as a function of PC_1 (top), PC_3 as a function of PC_1 (middle) and PC_3 as a function of PC_2 (bottom) for the various sites and experiments. The points for each site use the colour from Table 1 (small spheres are for 'before' - or unchanged - and large ones for 'after' modification).

4.3.3 Interpretation of the Principal Components

An initial interpretation of what each of the components might signify has been attempted, but we must be careful not to read too much into what has been essentially a preliminary analysis of the data. The following analysis will therefore have to be confirmed after a much larger dataset including a large variety of sites and surface types, and covering a wide range of conditions have been examined.

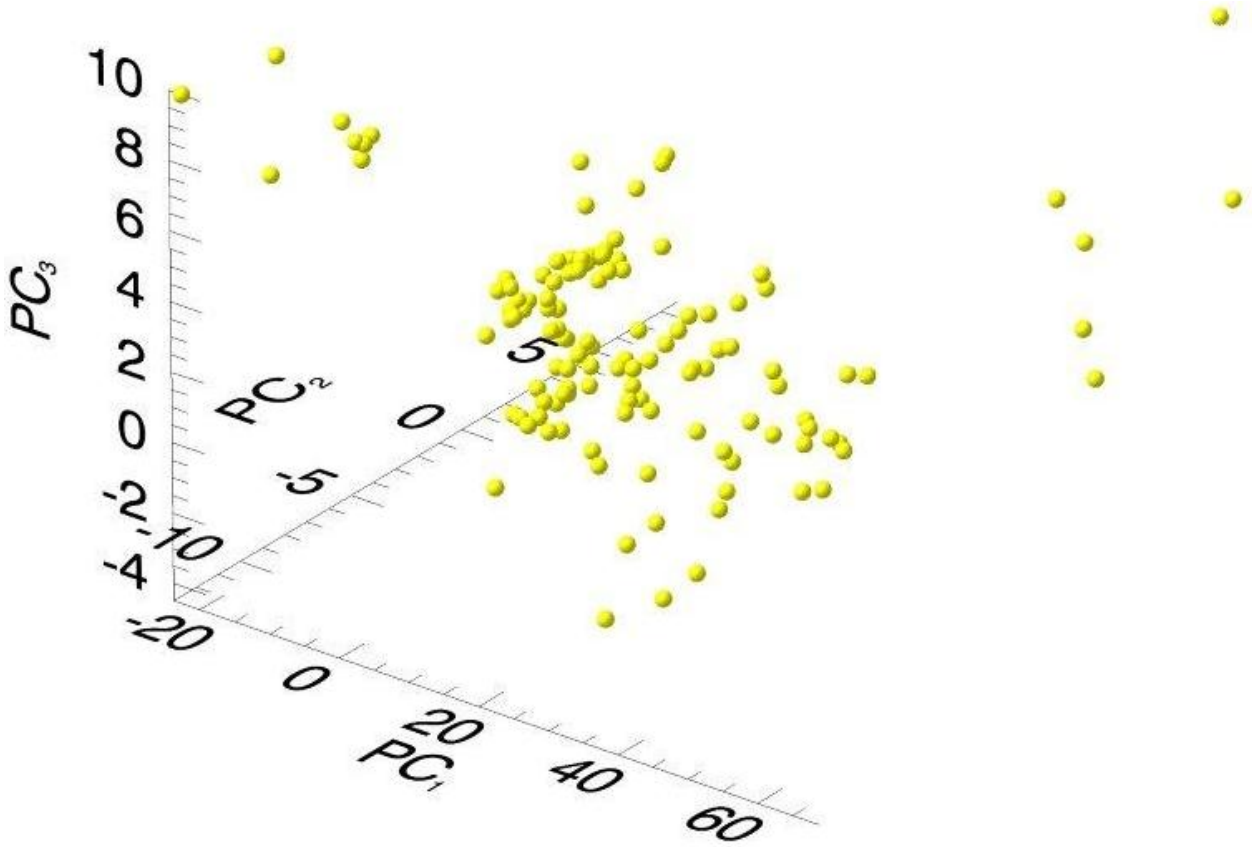

Figure 31: 3-D representation of the all the data in the PC_1-PC_2-PC_3 coordinate system.

On both the bi-plots (Figure 30) and the 3-D scatter plots (Figure 31) there are groups of points with highly correlated attributes, typically those labelled 1A and 1B (royal blue) or 3A and 3B (pink): these are from repeat surveys of Sites 1 and 3, where most of the surface was left unchanged between surveys, but in survey 1B some of the surface was masked with sand to reduce the texture depth, and in survey 3B some aggregate was removed from some small areas of the pavement to simulate surface disintegration.

Modifications to the characteristics of the pavement surface on Site 2 with the removal of loose aggregate significantly increased the value of PC_1 as the defect 'proportionally' affected a larger surface area where the regions marked with the chalk represent a small portion of the images): this component potentially carries information about the *severity* of the fretting.

PC_2 has a large contribution from parameter *Spk* which measures the roughness depth of the peaks in the data. The behaviour of PC_2 on sites where sand was sprayed on the surface of Site 1, and others where aggregate was removed from small areas in Site 3, suggests that PC_2 is related to the depth of peaks in the data, and that by removing aggregate the absolute value of this principal component will increase in magnitude to reflect the increase in the proportion of data which is from holes, or missing aggregate.

The 3rd principal component, PC_3, is strongly correlated with the mean density of furrows in the measured surface. Changes in this parameter from surfaces where sand was used to mask the surface texture suggest that this PC_3 parameter will fall on smoother surfaces, and, as a corollary to this, will increase on surfaces where the texture has got rougher. It is therefore expected that an increase in this parameter will be associated with an increase in the amount of missing aggregate on a surface. This was borne out by looking at the data from Site 3.

5 Detailed discussion of sites and main results

Various tests were carried out on a number of different sites, as detailed in Section 3.2. The key results of some of these are presented and discussed in the following sections.

5.1 Site 1 – SRS access road

Site 1 was located on an access road to the TRL Small Road System (SRS). This site had an HRA surface, in good condition, with a typical aggregate size of approximately 10mm. The surface at this site was in good condition at the time of measurement, but had to be swept clear of numerous fallen pine needles prior to collecting data. Figure 32 shows a relatively close-up view of the surface at Site 1.

Figure 32: Site 1 surface – as found.

Data was collected over the site in its as-found condition, and then finely textured sand was spread over the surface to fill in and mask some of the texture (Figure 33), before a subsequent data collection run was undertaken.

Figure 33: Site 1 surface showing sand used to mask texture.

Figure 34 shows surface data from two measurement passes over part of Site 1. The top image shows the measurements made with the site in its as-found condition; the lower image shows the same portion of Site 1 after sand has been added (main area of sand is highlighted with an ellipse).

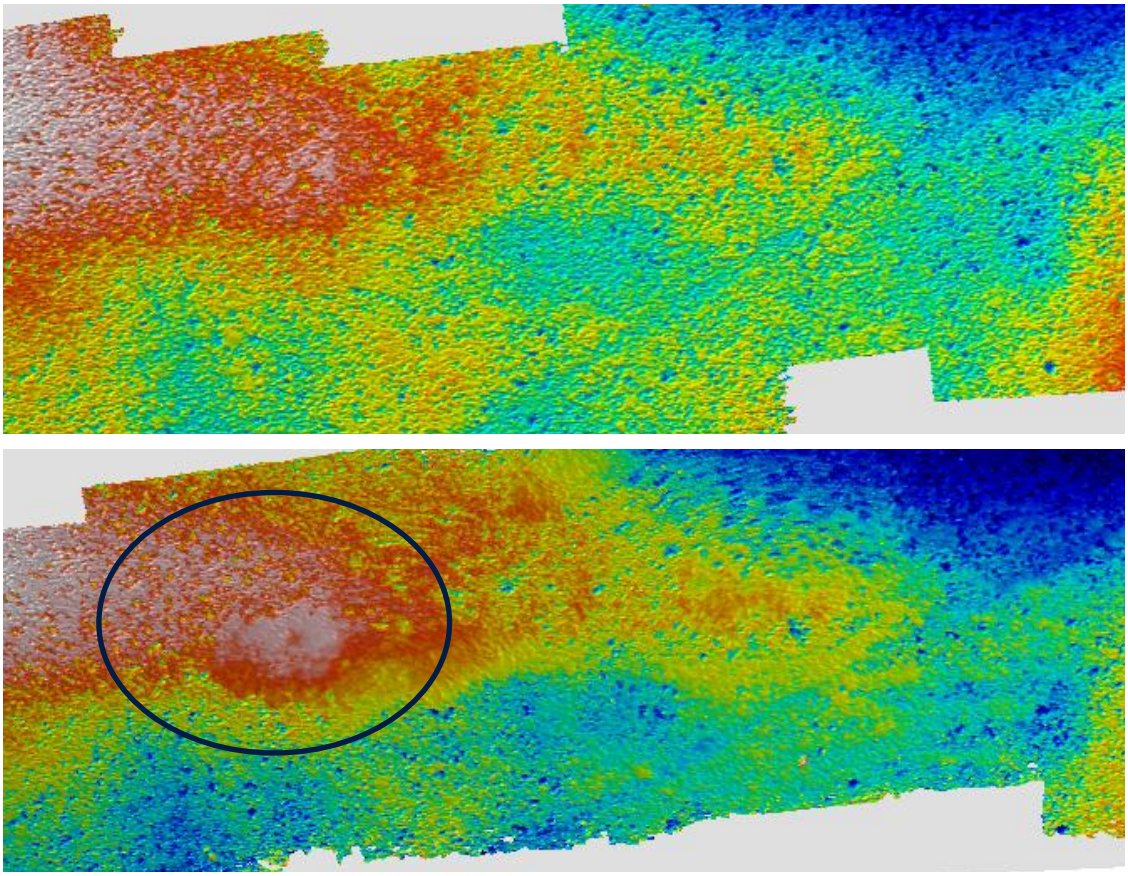

Figure 34: 3-D measured surfaces on Site 1 from before (top) and after (bottom) the addition of sand.

5.2 Site 2 – Tennis courts car park

Site 2 was located near the car park beside the TRL tennis courts (Figure 35). The area chosen for the trial was an old HRA surface in very poor condition, with lots of loose and missing aggregate (as shown in Figure 36). As before, the surface was prepared for survey (marked and swept) before collecting data on the surface. The loose aggregate was then removed from part of the site (Figure 37) and it was surveyed again.

Figure 35: General overview of Site 2 and equipment.

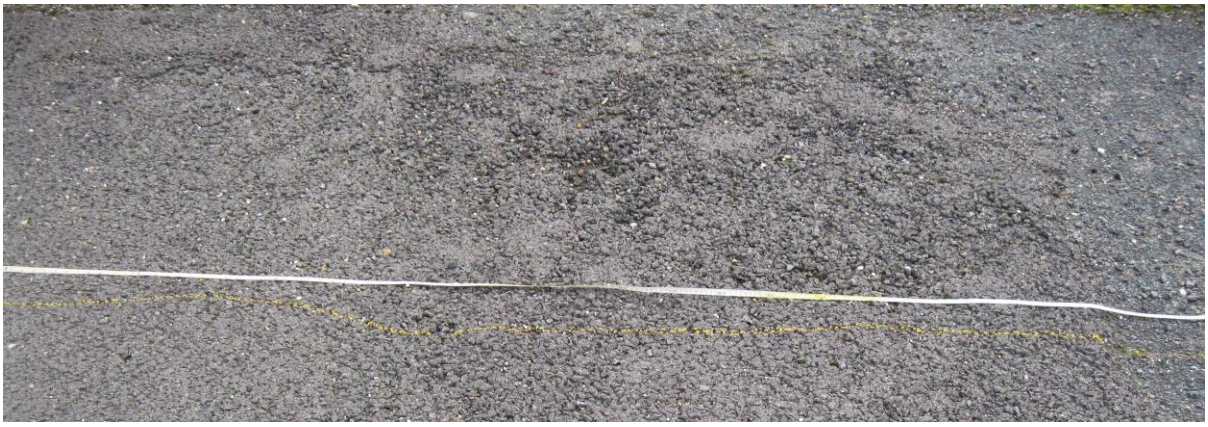

Figure 36: Site 2 surface before removal of loose aggregate.

Figure 37: Site 2 surface after removal of loose aggregate (note that the picture was taken from a different point of view).

Figure 38 shows the measured 3-D surface of part of the site from two different survey runs, where no artificial change has been introduced to the surface. The two images can be seen to be well aligned, with a number of detailed features visible in both datasets. There are no visually obvious changes in the condition of the surfaces shown in Figure 38.

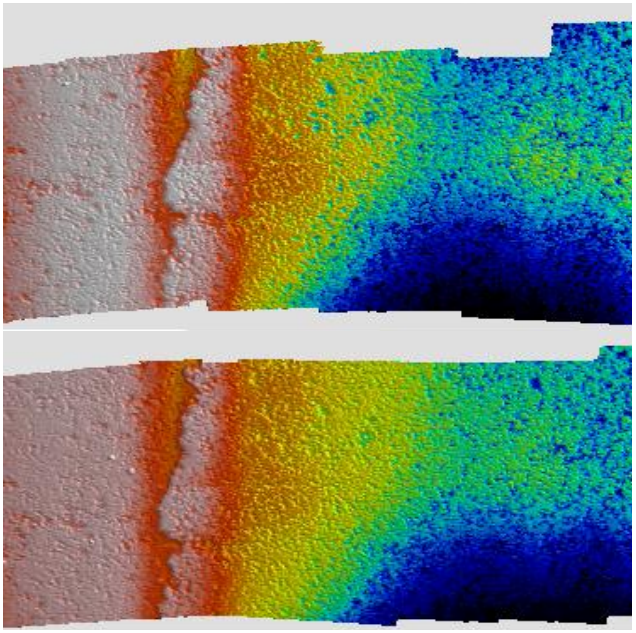

Figure 38: Images showing 3-D scans of part of Site 2 where no change has occurred.

Figure 39 shows two 3-D surfaces from another part of Site 2. In this case a lot of the loose aggregate present on the surface has been removed prior to the second survey being undertaken. This can be seen as an increase in the area of the darker colours in the lower image, signifying a larger area with higher depth measurements.

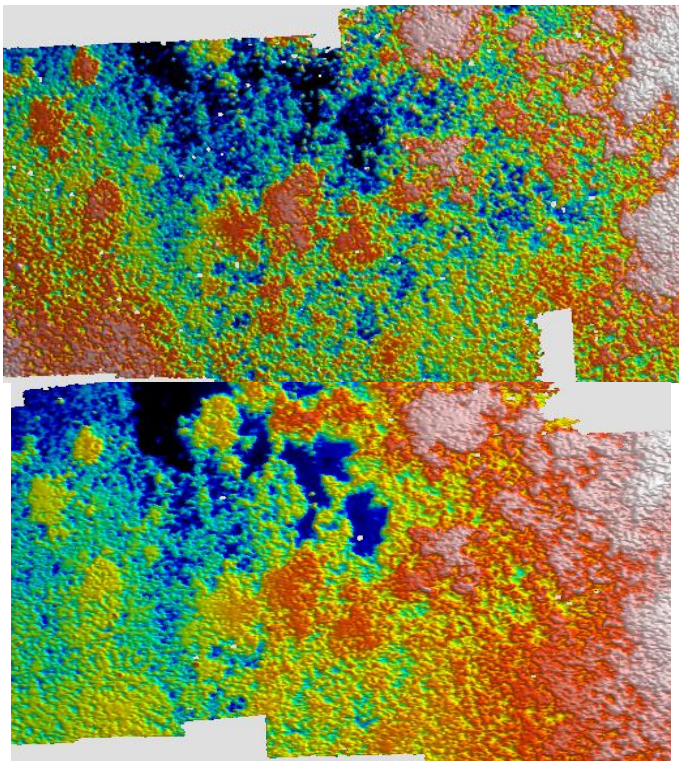

Figure 39: Images showing 3-D scans of part of Site 2 before (top), and after (bottom), removal of loose aggregate.

The first three Principal Components (PC_1, PC_2 and PC_3) are shown for Site 2 in Figure 40.

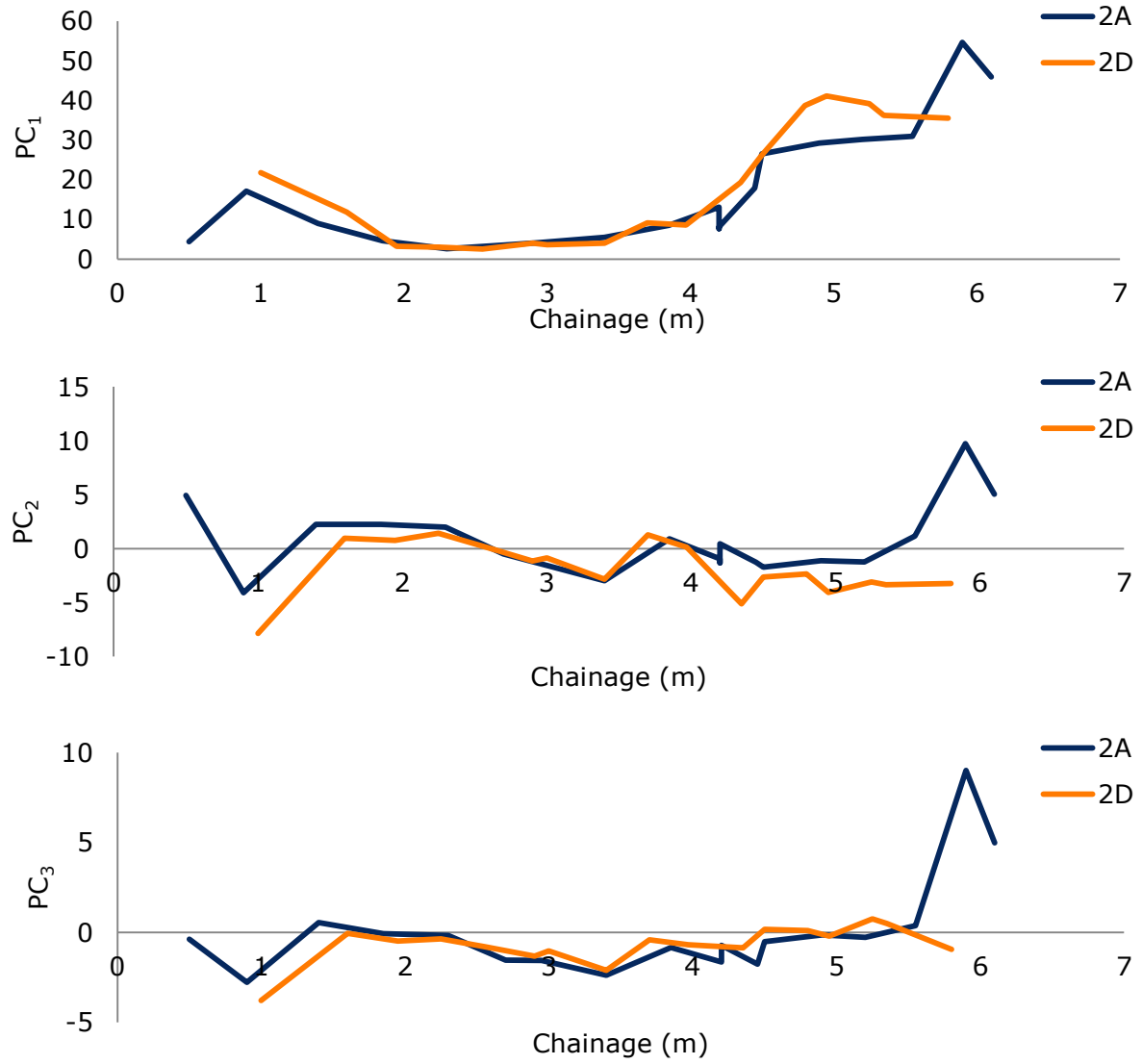

Figure 40: First three Principal Components (*PC_1*, *PC_2* and *PC_3*) for Site 2.

The area where loose aggregate was removed on Site 2 was between approximately 4.5m to 6m along the site. We can see, in all three principal components, that the before and after data shows very little change in the measurements on the site up to this point. We can also see that the first two principal components, and in particular *PC_1*, start to show some change in the condition from about 4.5m onwards.

5.3 Site 3 – TRL staff car park

Site 3 located within the TRL staff car park (Figure 41) is a Thin Surfacing System, with a typical aggregate size about 8mm. The site was in better initial condition than the Site 2.

As before, the site was prepared, swept, marked and then data was collected along its length. The site preparation this time included marking on two 150mm × 150mm areas on the surface. The surface within these marked areas was subjected to some forced deterioration before undertaking a second survey pass.

Figure 41: General overview of Site 3 and equipment.

Figure 42 is from part of Site 3, measured before introducing any change to the surface, along with an extracted profile from an area where change would later be introduced. Figure 43 shows the same part of Site 3 following the forced deterioration of the areas within the marked squares, and an extracted profile. The deterioration mechanism involved removing two or three individual stones, leaving the rest of the surface virtually unchanged.

Note: a different colour map has been used in Figure 42 and Figure 43 than in most other figures. This has been chosen purely for reasons of clarity of display and interpretation.

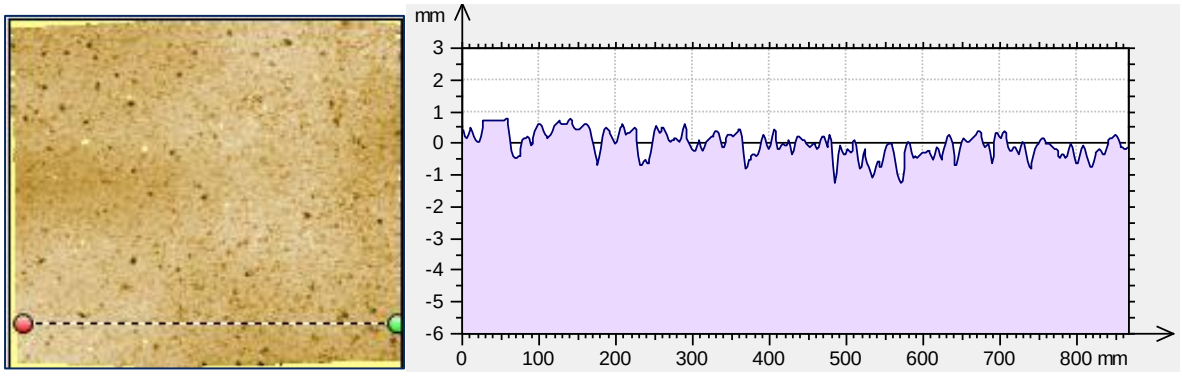

Figure 42: Surface and extracted profile from 7.5m along Site 3 before forced deterioration.

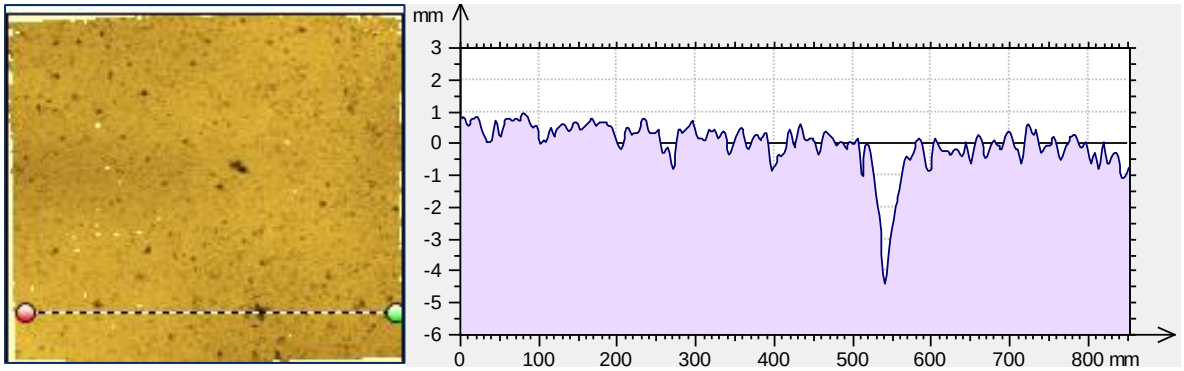

Figure 43: Surface and extracted profile from 7.5m along Site 3 after forced deterioration.

The profiles shown on the right of Figure 42 and Figure 43 are very similar, apart from at a horizontal position of approximately 550mm, where the damage can be clearly seen as a negative spike with a depth of about 4mm and a width of approximately 25mm: this is where 3 or 4 individual stones were removed using a hammer.

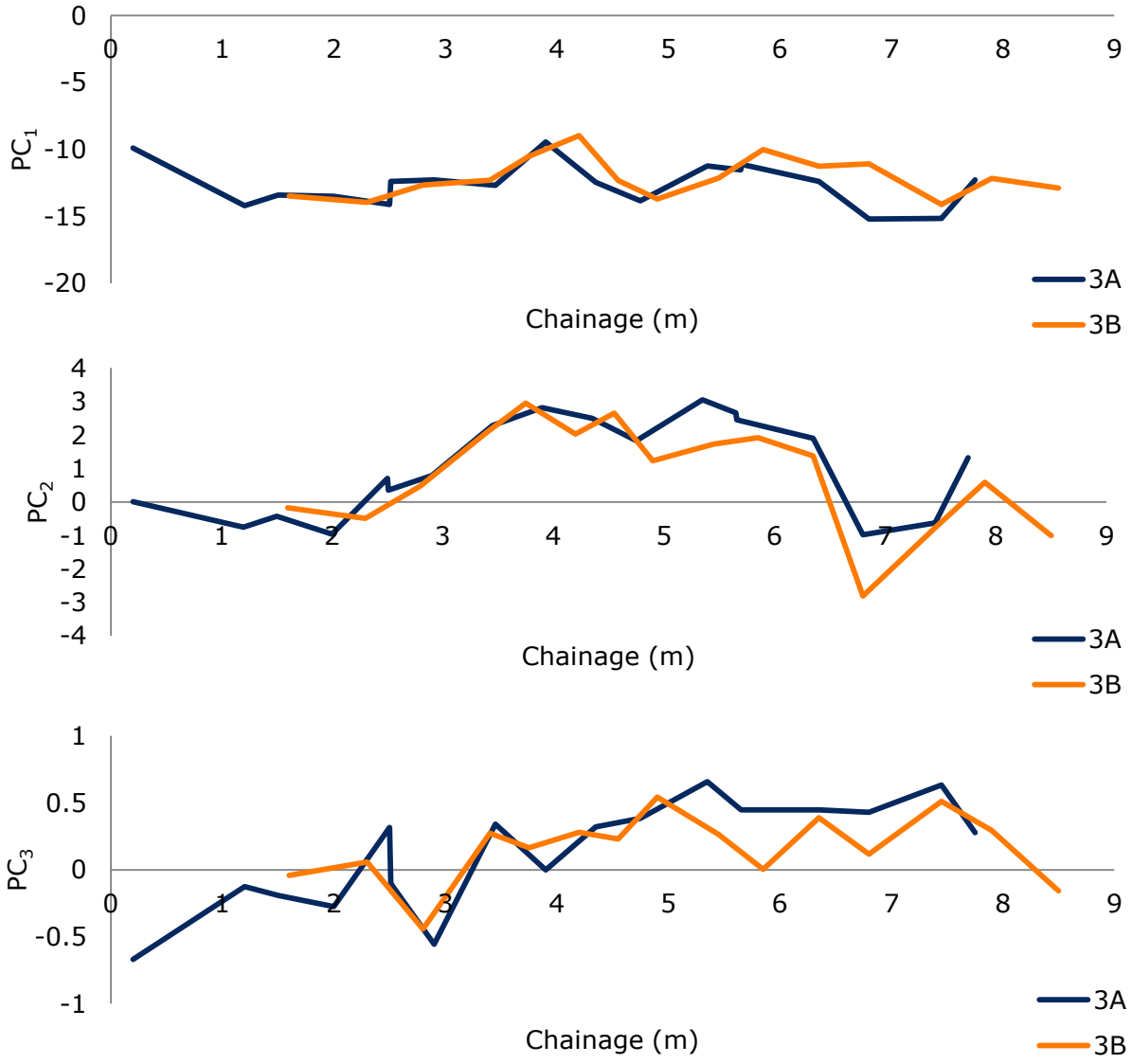

Figure 44: First three Principal Components (PC_1, PC_2 and PC_3) for Site 3.

Figure 44 shows the first three principal components for the data on Site 3. It can be seen in these plots that the principal components generally follow the major trends along the site, although there are a number of localised differences. Site 3 was subjected to some forced removal of aggregate in a couple of small areas approximately 7.5m and 8m along the site. These changes do not seem to have affected the principal components strongly enough to be apparent on these plots.

Figure 45 shows the principal components for four small areas (each approximately 150mm × 150mm square) within Site 3. Two sets of measurements were made on these four areas, one before any change happened and one after. The forced change involved removing some aggregate from two of the four studied areas (areas *i* and *ii*). The other two areas (*iii* and *iv*) were unchanged between surveys.

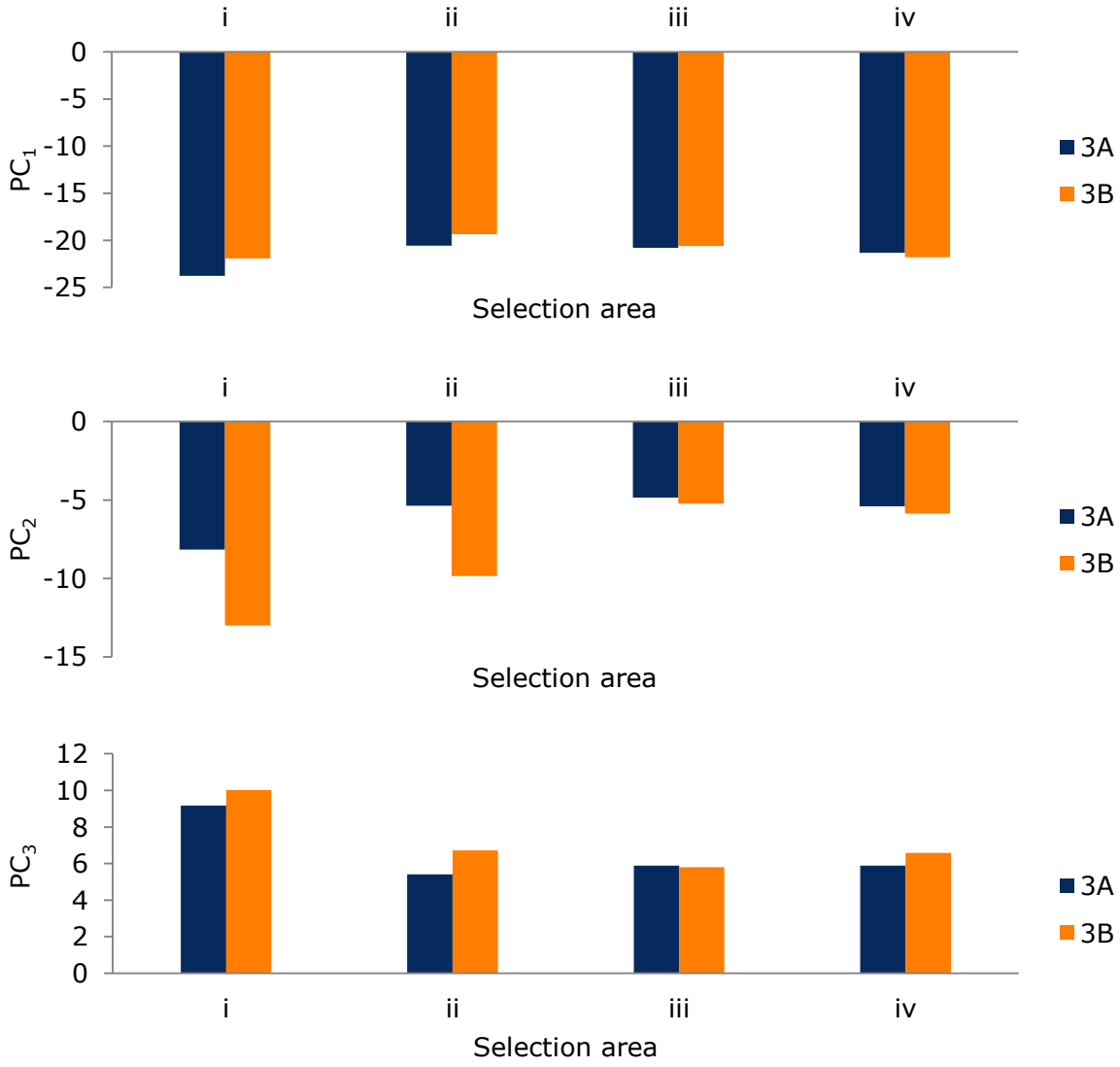

Figure 45: First 3 principal components on four small sample areas within Site 3.

It is clear from Figure 45 that the principal components calculated on samples *i* and *ii* have changed significantly between the before (3A) and the after (3B) measurements. The modifications in PC_2 (and, to a smaller extent, PC_3) are particularly noticeable. The principal components calculated on the data measured in the unchanged areas (*iii* and *iv*) show far smaller changes.

6 Conclusions

Earlier research on the detection of fretting, exploiting single or multiple line texture profile data, has developed algorithms which allow the identification of surface disintegration at the network level, where it is present at a high level of severity. However, engineers need to detect the onset of the deterioration, before it reaches this point, so that preventive, rather than reactive, maintenance can be carried out.

This phase of the research has therefore concentrated on the development of a method to enable engineers to identify the early stages of surface disintegration. The research has been based upon the assumption that high-resolution 3-D profile measurements could be used to detect the loss of stone in road surfaces, and that the change in the profile could be used to assess the deterioration. We have demonstrated the potential for high-resolution profile data in this application.

A 3-D profile measurement system has been commissioned on a semi-mobile platform to collect very high-resolution surface profile data on test sites. Manual analysis of the data has shown that changes in surface condition can be identified in the 3-D images. We have also proposed several statistical measures and a number of volumetric parameters which were found to be appropriate to quantify differences in condition. Principal component analysis techniques have been successfully employed to reduce the number of parameters which need to be considered in making assessments of the surface down to three key indicators or components.

Visual assessment of data collected using a high-resolution 3-D imaging system is able to identify the differences in the measured surfaces of different surface types, and the data can be quantified and parameterised to measure changes in the surface condition. However, there are still many hurdles to overcome to get from here to a routine traffic-speed system.

7 Recommendations

There is a need to better understand how surface disintegration starts and develops. This can be tackled by monitoring network sites which are about to fail, or replicating the deterioration of test surfaces in a laboratory and collecting high-resolution measurements and reference data at regular intervals over a period of time. This could be used to evaluate the change both numerically and visually, with a view to understanding the very early stages of deterioration curves associated with surface disintegration. This will help inform future developments and define minimum data resolution and sensitivity requirements for routine network survey equipment.

Work should also be undertaken to investigate ways of automatically aligning data from successive scans, and on the development of suitable algorithms for detecting changes in surface condition which may be indicative of surface disintegration.

From a practical point of view modifications could be made to improve data acquisition with the mobile platform, for instance by increasing the clearance (with the addition of brushes, bigger wheels, etc.) which would make the system easier to manoeuvre and operate on uneven ground.

Acknowledgements

This work has been carried out in the Technology Development and Quality Assurance Group of the Infrastructure Division of the Transport Research Laboratory, supported by staff from Jacobs Engineering UK Ltd. The authors would like to thank all those involved in the data collection and processing, and would also like to express their gratitude for the support of Donald Burton and Colin Christie at the Highways Agency.

References

Department for Transport, 2012. *Prevention and a better cure - Potholes review,* London: Department for Transport - Highways Maintenance Efficiency Programme.

Hall, K., Correa, C., Carpenter, S. & Elliot, R., 2001. *Rehabilitation Strategies for Highway Pavements,* NCHRP Web Document 035, Project C1-38.

Iaquinta, J., Furness, G., Nesnas, K. & Wright, A., 2008. *Evaluation of the condition of rigid pavements - semi-automated assessment of surface features. CPR 053,* Crowthorne: TRL Ltd.

International Organisation for Standardization, 1997. *ISO 13565-2.*

International Organization for Standardization, 2012. *ISO Standard 25178-2.*

McRobbie, S., Iaquinta, J. & Wright, A., 2011. *Assessment of pavement Surface Disintegration at Traffic Speed - Phase 1 status report,* Crowthorne: TRL Ltd.

McRobbie, S. et al., 2012. *Development and validation of algorithms for the automatic detection of fretting based on multiple line texture data, PPR628,* Crowthorne: TRL Ltd.

McRobbie, S. et al., 2010. *Developing New methods for the Automatic Measurement of Raveling at Traffic-Speed.* Nagoya, Japan.

McRobbie, S. et al., 2008. *Assessment of surface ravelling using traffic speed survey techniques.* Potoroz, Slovenia.

Pearson, K., 1901. On lines and planes of closest fit to systems of points in space. *Philosophical Magazine,* 2(11), p. 559–572.

Scott, P. et al., 2008. *Measuring surface disintegration (ravelling or fretting) using traffic speed condition surveys.* Calgary, Canada.

van Ooijen, W., van den Bol, M. & Bouman, F., 2004. *High-speed measurement of ravelling on porous asphalt.* Toronto, Canada.

Appendix A Surface texture parameters

Many of the following surface and volumetric parameters are derived using the Abbott-Firestone Curve (shown in Figure 46). A brief description of this is provided here to help understand the parameters.

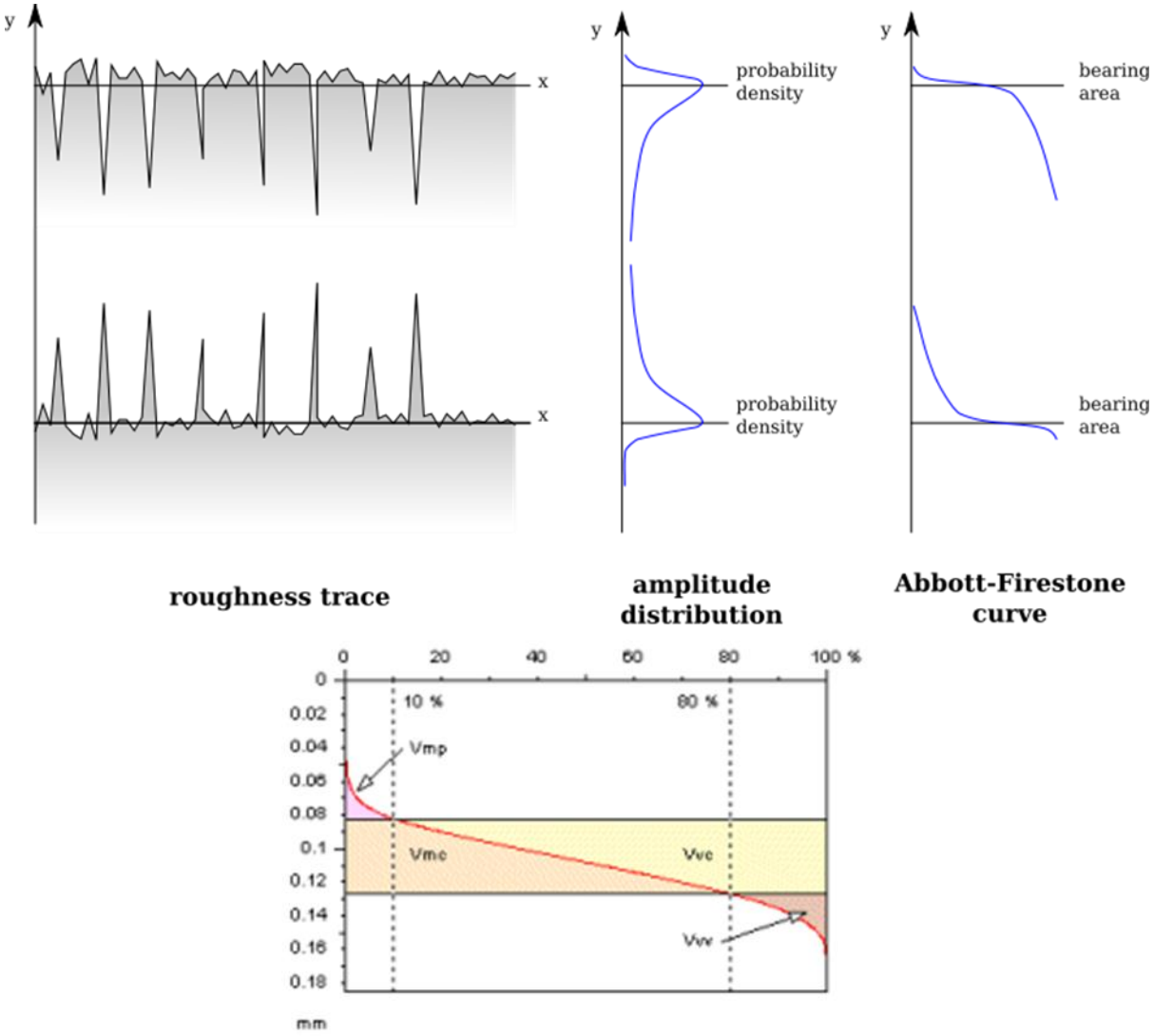

Figure 46: Abbott-Firestone curve. © Emok/ Wikimedia Commons / CC-BY-SA-3.0

Two bearing ratio thresholds are defined (the vertical lines). In this illustration these ratios are 10% and 80%. The first threshold, p_1 (in this case 10%), is defines the cut level c_1 (where the first bearing ratio threshold line crosses the curve). The second threshold, p_2, defines the second cut level, c_2 (where the second bearing ratio threshold line crosses the curve).

The following parameters are then calculated:

- *Vmp*: Volume of material in region above c_1 (peaks of surface material).
- *Vmc*: Volume of material in main body or kernel of surface, between c_1 and c_2.
- *Vvc*: Volume of void in kernel, between c_1 and *c*2.
- *Vvv*: Volume of void in surface valleys, at depths below c_2.

Sq – Root mean square height

The Root mean square height (measured in mm) gives a value for the mean height of a surface profile, relative to a flat plane through the mean height of the surface.

Ssk – Skewness

The skewness of a parameter (which is a dimensionless value) relates to the symmetry of a distribution and reflects the symmetry of the distribution of height measurements. A negative value for *Ssk* indicates a flat surface with lots of indentations when a positive *Ssk* indicates a flat surface with lots of peaks present (negatively and positively textured surfaces respectively).

Sku – Kurtosis

The kurtosis of a surface (dimensionless) is related to how peaked or flat a distribution is and this parameter reflects how evenly spread the measured profile heights are.

Sp – Maximum peak height

The maximum peak height of a 3-D surface (reported in mm) is the maximum height of the measured profile relative to a flat plane through the mean of the measured profile heights.

Sv – Maximum pit height

The maximum pit height is the depth (in mm) between the mean plane and the deepest valley in the surface profile.

Sz – Maximum height

The maximum height (in mm) of a profile point in the sample differs from *Sp* as this measures the maximum depth from peak to valley, whereas *Sp* measured the maximum height above the mean plane.

Sa – Arithmetical mean height

The Arithmetical mean surface roughness height (expressed in mm) is given by the sum of all height values in a surface divided by the number of values.

Smr - Areal material ratio

This parameter (expressed as a percentage) is the ratio of the area of the material at a specified height *c* (cut level) to the evaluation area. This requires setting a threshold value (*c*) which can be calculated with reference to the mean plane of the surface, or the peak height.

In the present analysis we looked at a height 10μm below the peak height of the surface.

Smc – Inverse areal material ratio

This parameter is closely related to the *Smr* parameter, but is reported as the height (*c*) at which a given areal material ratio *p* is satisfied. The height is calculated from the mean plane.

For example the previous parameter, *Smr*, shows the amount of the surface which is at a given height above the mean plane. This parameter, *Smc*, shows the height at which a specified amount of the surface is, with respect to the mean plane.

In our analysis we looked for the height at which we found 10% of the area.

Sxp – Extreme peak height

This Extreme peak height parameter (expressed in mm) is closely related to the previous ones, but is calculated for two material ratios. It expresses the difference in height between the *q*% and *p*% material ratio. This parameter must be configured with two thresholds entered in %.

Sxp = Smc(q%) - Smc(p%)

In our analysis we used values of 50% for p, and 97.5% for q.

Vm – Material volume

Vm is a volumetric expression of the 2-D surface parameter *Smc* (detailed above). This parameter (expressed in mm) shows the volume of the material at a material ratio *p* and is defined by Equation 1:

$$Vm(p) = \frac{\kappa}{100\%}\int_0 [Smc(p) - Smc(q)]dq$$

Equation 1: Definition of Vm.

Where *p* and *q* are the two material ratios, and κ is a constant to convert the parameter to mm^3/m^2.

Vv – Void volume

The Void volume (expressed in mm) is another volumetric expression of the 2-D surface parameter *Smc* (detailed above). This parameter shows the volume of the voids at a material ratio p.

$$Vv(p) = \frac{K}{100\%}\int_p^{100\%} [Smc(p) - Smc(q)]dq$$

Where *p* and *q* are the two material ratios, and *K* is a constant to convert the parameter to mm^3/m^2.

Equation 2: Definition of Vv.

Vmp – Peak material volume

This parameter expresses the volume of measured material in the peaks, between 0% material ratio and a defined material ratio *p*, calculated in the zone above c_1 (see above for explanation of Abbott-Firestone curve, and what c_1 is).

In this analysis we used a p value of 10%.

Vmc – Core material volume

Volume of material in the core or kernel (expressed in mm^3/mm^2) between two material ratios *p* and *q* (in %), calculated in the zone between c_1 and c_2 (see above for explanation of Abbott-Firestone curve, and what c_1 and c_2 are).

Vmc = Vm(q) - Vm(p)

In this analysis we used p=10%, and q=80%.

Vvc – Core void volume

The volume of missing material, or void in the main body of the surface (expressed in mm^3/mm^2) between two material ratios *p* and *q* (in %) is calculated in the zone between c_1 and c_2 (see above for explanation of Abbott-Firestone curve, and what c_1 and c_2 are).

$$Vvc = Vv(p) - Vv(q)$$

In this analysis we used p=10%, and q=80%.

Vvv – Pit void volume

Vvv is the volume of void in the valleys (expressed in mm^3/mm^2) between a material ratio *p* (in %) and 100% material ratio, calculated in the zone below c_2 (see above for explanation of Abbott-Firestone curve, and what c_2 is).

$$Vvv = Vv(p)$$

In this analysis we used p=80%.

The **wavelength** and **amplitude** parameters are calculated from the averaged power spectral density analysis of the surface. The reported values are those from the midpoint of the selected display. These were not fully explored during the analysis phase of this project.

It is possible to identify all the **furrows** in a surface. These can be characterised by their depth and position, and enable several different analyses such as:

Maximum depth of furrows

This reports the maximum depth (in mm) of the detected furrows within the surface.

Mean depth of furrows

This reports the mean depth (in mm) of all detected furrows within the surface and gives some indication of the mean texture depth on the surface.

Mean density of furrows

The mean density of furrows (in mm^{-1}) describes how closely spaced the detected furrows are in the surface. This is an indicator which is correlated to the aggregate size on the surface – smaller aggregate increase the density of the furrows; larger aggregate, or missing aggregate decrease the furrow density.

Thresholds (c_1, c_2, c_2-c_1)

c_1 and c_2 (expressed in mm) are the cut levels below which a defined material ratio lies within the surface, and are found using the Abbott-Firestone curve. Parameter c_1 is the lower cut level. Below this height on the surface material lie the troughs of the valleys. Parameter c_2 is the upper cut level, above which are found only the tops of the peaks of the positively textured elements of the surface. The parameter c_2-c_1 gives a quantified indication of the size of the main core, or kernel of the material. This shows the range of texture depths measured within the surface, excluding the very highest or lowest extremities, and will be much smaller on a uniformly textured surface than on a surface which is showing large texture variations or signs of distress.

In this analysis we set c_1 to cut at the 10% level, and c_2 to cut at the 80% level.